

Bayesian Belief Updating of Spatiotemporal Seizure Dynamics

Gerald K Cooray^{1,2}, Richard Rosch^{2,3}, Torsten Baldeweg³, Louis Lemieux⁴, Karl Friston², Biswa Sengupta²

¹Clinical Neurophysiology, Karolinska University Hospital, Stockholm, Sweden.

²Wellcome Trust Centre for Neuroimaging, Institute of Neurology, University College London, UK.

³Developmental Neuroscience Programme, Institute of Child Health, University College London, UK

⁴Department of Clinical and Experimental Epilepsy, Institute of Neurology, University College London, UK

Correspondence to: Gerald K Cooray, Wellcome Trust Centre for Neuroimaging at UCL - 12 Queen Square - London - WC1N 3BGUK. E-mail: gerald.cooray@ki.se. Phone: +44 7518 435676

Abstract

Epileptic seizure activity shows complicated dynamics in both space and time. To understand the evolution and propagation of seizures spatially extended sets of data need to be analysed. This requires efficient methods of inference. We have previously described an efficient filtering scheme using variational Laplace that can be used in the Dynamic Causal Modelling (DCM) framework to estimate the temporal dynamics of seizures recorded using either invasive or non-invasive electrical recordings (EEG/ECoG). In this note, we present a method to analyse the spatiotemporal dynamics of seizures. Spatiotemporal dynamics are modelled using a partial differential equation – in contrast to the ordinary differential equation used in our previous work on temporal estimation of seizure dynamics (Cooray et al 2015). We provide the requisite theoretical background for the method and test the ensuing scheme on simulated seizure activity data and empirical invasive ECoG data. The method provides a framework to assimilate the spatial and temporal dynamics of seizure activity, an aspect of great physiological and clinical importance.

Key Words: Dynamical Causal Modelling (DCM), Epileptic networks, Epilepsy, Seizure Activity, EEG/ECoG.

Introduction

Epilepsy is a chronic disorder characterized by heterogeneous and dynamic pathophysiological processes that lead to an altered balance between excitatory and inhibitory influences at cortical level (Engel, 1995). About 20% of patients with primary generalized epilepsy and up to 60% of patients with focal epilepsy do not respond adequately to antiepileptic drugs and develop pharmacoresistant epilepsy. Some of these patients may benefit from surgical treatment based on the resection of a notional epileptogenic zone; defined as the “minimal area of cortex that must be resected to produce seizure-freedom” (Engel, 1993, Vitikainen et al., 2013).

The gold standard for locating the epileptogenic zone is invasive neurophysiological recordings. Electrical activity of the cortex can be measured using macroscopic electrodes placed directly on the surface of the cortex (electrocorticography, ECoG) or using depth electrodes stereotactically placed at specific points within the cerebral cortex. These recordings have high time resolution (of approximately 1-5ms) allowing for the detection of fast neuronal dynamics. Moreover, as the volume of sensitivity of the invasive electrodes is usually approximately 1cm^3 , a comparatively high spatial resolution is possible, if many electrodes are used to sample the cortical activity (Asano et al., 2005). For ECoG recordings a grid of electrodes is used to cover a cortical area of clinical importance. This methodology allows for a sampling of cortical seizure activity, disclosing the spatiotemporal dynamics and facilitating the detection of rapid neuronal dynamics; including the generation, spread and termination of electrographic seizure activity.

Quantitative analysis of the temporal aspect of cortical activity was introduced by Wilson and Cowan, where population activity of neurons – following Hodgkin-Huxley dynamics – was summarised using methods from statistical physics (Wilson and Cowan, 1972, 1973). The neural mass models they proposed provided computationally tractable ways of modelling cortical activity over time, especially in the form later introduced by Jansen and Rit (Jansen and Rit, 1995). Neural mass models are nonlinear, allowing many possible routes to seizure activity: seizure initiation has been modelled using nonlinear phenomena such as bifurcations (Breakspear et al., 2006, Grimbert and Faugeras, 2006, Blenkinsop et al., 2012, Nevado-Holgado et al., 2012, Jirsa et al., 2014) or multistability (Lopes da Silva et al., 2003, Benjamin et al., 2012). Variation in the parameters of neural mass models has also been used to model seizure activity and inferences about these changes can be made using Bayesian statistics;

including stochastic filtering or genetic algorithms (Wendling et al., 2005, Schiff and Sauer, 2008, Ullah and Schiff, 2010, Blenkinsop et al., 2012, Nevado-Holgado et al., 2012, Freestone et al., 2014).

The neural mass formulation models the entire population activity as a lumped mass without taking into account any spatial spread. Although neural mass models have been used extensively to study the temporal dynamics of seizures, their inherent assumptions preclude an in depth analysis of spatiotemporal dynamics. Other neuronal models, such as neural field models, have explicitly included the spatial aspects of neuronal activity. However the comparatively high computational complexity of these models makes inference under such models very difficult.

Neural field models have been studied since the seminal work of Wilson and Cowan, and Amari to name a few (Wilson and Cowan, 1973, Amari, 1977). The mathematical foundations of such fields have been thoroughly investigated by Amari (Amari, 1977). These models have been used to investigate several different types of physiological and pathological brain activity (Jirsa and Haken, 1996, Golomb and Amitai, 1997, Jirsa and Kelso, 2000, Rennie et al., 2000, Liley et al., 2002, Robinson et al., 2002, Rowe et al., 2004, Coombes, 2005, Robinson, 2006, Coombes et al., 2007, Deco et al., 2008). The neural mass model is replaced by an integro-differential equation. These models include the effect of spatial signal transfer on cortical activity and have been modified to improve tractability of model inversion (Schiff and Sauer, 2008, Pinotsis et al., 2012, Moran et al., 2013).

The neural fields described above model spatial dynamics of cerebral activity due to direct connectivity among neurons at different positions on the cortex. These connections are usually considered to be constant over the timescale of a single seizure, but several studies have suggested that during seizures there are changes in intra- and extracellular factors such as electrolytes, metabolites and neurotransmitters. Mediated through the local interaction between glial and neuronal cells many of these factors will change the intrinsic dynamics of the cortex (Ullah et al., 2009, Frohlich et al., 2010, Wei et al., 2014a).

We argue in this note that a simplified spatiotemporal field can model the temporal and spatial behaviour of seizure activity. To contain the model's complexity and allow inference on our model, we decouple fast temporal activity from slower spatiotemporal fluctuations. This adiabatic assumption respects the biology based on the diffusion or transport of extracellular or intracellular factors as described above – and their interaction with synaptic connectivity of

cortical neurons, which is assumed to produce fast temporal activity. The slowly varying field will be a representation of the mixture of the slowly varying changes that affect neuronal activity, such as extracellular electrolytes, metabolites and O₂ concentration. Thus the model studied here differs from the classical neural fields – the spatial dynamics will be caused by slow changes in extra/intracellular factors during seizures. In effect, this paper introduces a novel application of dynamic causal modelling based upon a hierarchical DCM, with first level (fast) spectral activity and second level (slow) spatial dynamics. Crucially, this hierarchical model enables (slow) dynamics to generate fluctuations in the parameters generating (fast) neuronal activity.

The model will be formulated within the Dynamic Causal Modelling (DCM) framework. DCM allows for the inversion fitting of generative models, where inferences can be made about the neuronal architectures that underlie physiological signals (Stephan et al., 2007). Within the modelling of fMRI and EEG activity DCM has found wide applicability (David et al., 2008, Moran et al., 2011a, Moran et al., 2011b, Moran et al., 2011c, Friston et al., 2012). DCM generally rests upon the variational Bayesian inversion of biophysical generative or forward models. The evidence for different models generating the same empirical data can be estimated, enabling a model and thus a hypothesis comparison. Posterior estimates of the parameters of the best model (or their Bayesian model average) then provide quantitative and physiologically grounded explanations for the measured physiological signals.

Method

The model used in this study comprises a neural field (where electrographic activity depends not only on time but also location in space, i.e. location in the cortex). A field equation is in general described with a set of partial differential equations that contains derivatives over multiple dimensions (here: time and space), in contrast to the ordinary differential equations of neural mass models that only contain derivatives with respect to time.

These models are usually less amenable to real/complex analysis and are numerically challenging to invert. To construct an invertible generative model, we partition our model into hidden states/parameters that are not explicitly (conditionally) dependent on spatial location and parameters that depend on spatial location. Furthermore, we assume that the temporal fluctuations of the spatially dependent subset will be several orders slower than the

temporal dynamics of the hidden states/parameters that are conditionally independent of spatial location. In other words, we will have neural mass models positioned at every point of the cortex, where some of the parameters of the neural mass model will be governed by a partial differential equation that includes spatial dependencies, i.e. a parameter field equation. Parameters not governed by spatial dynamics will be sampled from a Gaussian distribution.

From a biological point of view, this model could represent the activity created by cortical neurons under the influence of slowly diffusing extracellular factors such as interstitial electrolytes, O₂ concentration and neurotransmitters. These factors have been shown to affect cortical activity during seizures and some are governed by the interaction between glial and neuronal cells (Grafstein, 1956, Fetziger and Ranck, 1970, Kager et al., 2000, Nadkarni and Jung, 2003). A realistic but computationally expensive model capturing these effects would be to use e.g. a reaction-diffusion equation (Cornell-Bell et al., 1990, Finkbeiner, 1992, Loewenstein and Sompolinsky, 2003). For reasons of numerical efficiency we introduce the simplifying assumption that transport of electrolytes through extracellular medium or through glial cells is via passive diffusion.

The partition of the model described above is akin to an adiabatic elimination of the fast variables that are implicitly dependent on spatial location through the slower variables (Risken and Frank, 1996). The fast activity is governed by the following linearization of a neural mass model, a canonical microcircuit (CMC) as currently implemented in DCM (Moran et al., 2013, Bastos et al., 2015), see Appendix A.

$$\frac{dx}{dt} = A(\theta_i, \theta_{sp})x + u(\theta_e) \quad Eq. 1$$

- A is the Jacobian of the CMC around its steady point
- u is a random variable representing the external input to a specific part of the brain.
- θ_i are the parameters not explicitly governed by spatial dynamics. These would represent biophysical variables governing the activity at a point on the cortex.
- θ_{sp} are the parameters showing explicit spatial dynamics. These would represent slowly varying extracellular factors including the interaction of the glial cells and the neuronal cells.
- θ_e are the parameters governing the unmodelled extrinsic (afferent) input to a cortical column or neural mass.

- x is the (hidden) state that represents the average membrane potentials and currents of the different subpopulations of the cortical column

The measured local field potential is approximated by a linear mapping (L) from the hidden state (i.e., depolarisation) of the neuronal populations x :

$$y = Lx \quad \text{Eq. 2}$$

We model the spatially dependent parameters be governed by a simple diffusion law (or Fick's law, with a diffusion coefficient of $k=1$)

$$\frac{d\theta_{sp}}{dt} = k\nabla^2\theta_{sp} \quad \text{Eq. 3}$$

At this point we appeal to the assumption that the dynamics of the neuronal activity (x) compared to parameters ($\theta_i, \theta_{sp}, \theta_e$) are at least several orders of magnitude faster. This allows us to estimate neuronal activity as the steady state activity of Equation 1. We can then write the expected spectrum of the neuronal activity as a function of the parameters $\theta_i, \theta_{sp}, \theta_e$. This approach has been adopted in a similar setting (Moran et al., 2011c, Cooray et al., 2015b).

Our model of the spectra measured during discrete time intervals from the local field potentials (estimated over suitable windows, i.e. epochs that retain 95% of the total spectral power of the original data) is given by the following measurement model (Eq. 4) and a partial differential equation (Eq. 5):

$$y_k = H(\theta_i(t_k), \theta_{sp}(t_k), \theta_e) + r_k \quad \text{Eq. 4}$$

$$\frac{d\theta_{sp}}{dt} = \nabla^2\theta_{sp} + q(t) \quad \text{Eq. 5}$$

In the following equations sampling error $r_k \sim N(0, R_k)$ is sampled from a Gaussian distribution and $q(t)$ is defined as a white noise process (Eq.6). The diffusion equation is infinite dimensional making it difficult to solve analytically and numerically. However, we will approximate the partial differential equation using a finite set of eigenfunctions, $\varphi_i(x)$, and eigenvalues, λ_i , of the partial differential equation. This results in the following simplified set of equations (Sarkka et al., 2012, Solin, 2012):

$$y_k = H(\theta_i(x, t_k), \theta_{sp}(x, t_k), \theta_e(x, t_k)) + r_k \quad \text{Eq. 6a}$$

$$\theta_{sp}(t) \approx \sum c_i(t_k)\varphi_i(x) e^{-\lambda_i(t-t_k)} \quad \text{Eq. 6b}$$

$$c_i(t_k) = c_i(t_{k-1})e^{-\lambda_i(t_k-t_{k-1})} + q_i(t_{k-1}) \quad \text{Eq. 6c}$$

In the above equation $q_i(t_k) \sim N(0, Q_{i,k})$ is sampled from a random Gaussian variable. A similar idea has previously been presented in DCM of distributed electromagnetic responses where the cortical activity was parameterised using a set of local standing-waves of neural field models (Daunizeau et al., 2009).

The data generated by this model comprised windowed spectral data $\{y_{k,ij}\}$ from the i th row and the j -th column of any electrode array used to measure the electrographic activity sampled at time t_k . We estimate the parameters of our model in each time window using variational Laplace. The values in the next time window will be predicted using Equation 6, given the previous values. We can estimate an approximate solution to the above stochastic model using a simple form of Bayesian belief updating – as has been previously described (Cooray et al., 2015b).

Effectively, Equation 6 is an empirical (or hierarchical) Bayesian model that has two levels. The top (second level) has parameters or coefficients that control the amplitude of spatial basis functions (these are the eigenfunctions of a diffusion process). The generative model for these (second level) parameters is a simple autoregressive process. The first level (neuronal connectivity) parameters are generated at each point in space and time (from Equation 6b) and enter a first level model. The first level model is a standard DCM for cross spectral density (Moran et al., 2011c), which generates the observable (cross spectral) data at each point in time. The simple form for the second level model means that we can invert the hierarchical model by updating the second level parameters (coefficients) using Bayesian belief updating. In other words, we can take the first level parameter estimates from any epoch and evaluate a maximum likelihood estimate of the second level coefficients based on the spatial profiles of first level parameters. The maximum likelihood estimate is combined with a prior from the previous epoch. The resulting posterior then becomes the prior constraint for the next epoch – and so on.

In effect, applying the second level provides empirical prior constraints on the spatiotemporal evolution of first level parameters. The simplicity of the scheme is afforded by the adiabatic expansion that separates the fast dynamics (within-epoch) from the slow fluctuations (between-epoch) that are modelled by the second level. The amplitude of the random fluctuations in spatiotemporal dynamics determines the smoothness of the diffusion process and the degree to which between-epoch updates are constrained by previous estimates.

In summary, our Bayesian belief updating scheme estimates slowly varying parameters as follows:

- Window the data into suitable epochs (retaining 95% of the total spectral power)
- Estimate the posteriors of the parameters in the first epoch
- Replace the priors over the parameters in the next epoch with the posteriors of the previous multiplied with the appropriate decay factor ($e^{-\lambda_i(t_k - t_{k-1})}$, see Eq. 6c).
- Estimate the posteriors of the parameters in the next epoch
- Continue recursively for all epochs

Simulations

In this section, we compare the inferences based on simulated ECoG data generated by slowly varying parameters with the actual drifts of these parameters used to generate the spatiotemporal data. We simulated ECoG data with both one and two dimensional spatial dynamics, which are then inverted to compare the inferred spatial dynamics with the true values (ground truth). This is the usual approach to establishing the face validity of the model and its inversion; i.e., does the model fitting properly identify the generative architecture.

One-dimensional domain

Data was simulated where the slowly varying parameter (θ_{sp}) controlled the gain of excitatory connections in the canonical microcircuit. The spatial dynamics for this first simulation was given by a 1 dimensional diffusion equation. The diffusion of the parameter was calculated along a line with time dependent boundary conditions: see Appendix B for the equations used in the calculation. The boundary conditions on the line were set to zero at one end and to a Gaussian function of time at the other, i.e. the parameter varied smoothly from zero to one and then back to zero at one end (CF: a simulated source of extracellular fluctuations at a seizure onset zone). We calculated the diffusion of this parameter along the line using the adiabatic separation of variables above. The exact solution of the diffusion can be given by an infinite series of eigenfunctions to the diffusion equation and the *particular function* to the boundary conditions. As a final simplification – to construct a generative

model that permitted inference on the spatial dynamics of θ_{sp} – we projected our infinite dimensional solution to a finite dimensional subspace defined by the three principal eigenfunctions of the diffusion equation. We estimated the simulated response at five predetermined points along the line. The simulated data was used to invert the model described above. Figure 1 shows the spatial variation of the simulated data and the estimated parameters of the inverted model.

[Figure 1 A&B]

The simulated dynamics of θ_{sp} was sampled at five points from the origin using “virtual electrodes”. The spectral activity of the electrographic activity at each of these electrodes was evaluated (using Equation 1) using sequential 1000 ms time windows. The simulated activity showed time frequency plots that are similar to epileptic activity seen when measured using ECoG strips. Note the delay in the maximal seizure activity as distance from the origin (which represents the seizure onset zone) increased. This was related to the latency of changes in the excitability at each source, mediated by the slow spatiotemporal dynamics, see Figure 2. ‘

[Figure 2]

The quality of estimation of the spatiotemporal dynamics of the one dimensional simulation is reasonable; however, there is a mismatch for electrode position 1 and 2 (explained variation > 0.85). This is due to the eigenfunctions that were used to simplify the problem: they fulfilled Dirichlet boundary conditions, i.e. 0 along the boundaries; an infinite number (or very large number for numerical calculations) would be required to match the simulated spatiotemporal dynamics close to the boundary points. Alternatively, the diffusion equation could be solved using purely numerical techniques such as finite difference or finite element methods. These methods are computationally more intense but can, in principle, model almost any activity near the boundaries (Lui, 2012).

Two-dimensional domain

The above simulation was restricted to one dimension, which is unrealistic for modelling seizure spread across the human cortex. The previous simulation would most closely resemble the unusual case of the spread of seizure activity across a region of the brain along a plane wavefront. We therefore performed a more realistic simulation of seizure activity spreading

over the cortex: the simulated seizure was generated at a point and spread over the neighbouring two dimensional cortical surface. The spread of the seizure was modelled as the diffusion of an excitatory parameter diffusing from a central focus. This simulation generates electrographic activity of the sort seen in real seizures when recorded invasively, specifically focal seizures (Traub et al., 2010). In this simulation, we assumed a symmetric spread of the seizure, although it is straightforward to extend the simulation to a more realistic non-isotropic spread of seizure activity.

More specifically, we used the two dimensional diffusion equation with rotation invariant eigenfunctions, i.e. first and second order Bessel functions. For inversion, we mapped the dynamics onto a subspace of finite dimension generated by a small set of Bessel functions (7 terms were used in the present simulation), similar to the procedure for the one dimensional simulation, see Appendix B. The resulting (simulated) electrographic seizure activity was measured using a grid comprising 5 by 5 electrodes /placed such that the focus of the seizure activity was outside the grid to the top left. The spread of the excitatory parameter was simulated and used to generate the spectral response measured at the electrodes in the grid; see Figure 3. The resulting spectral responses were used to estimate the spatial dynamics of the excitatory parameter as above. The predicted data is shown in figure 4, which shows an excellent fit to the measured spectral activity (explained variation > 0.99). Furthermore, the inferred fluctuations of the excitatory parameter is nearly identical to the simulated dynamics (explained variation > 0.90), figure 5.

[Figure 3]

[Figure 4]

[Figure 5 A&B]

Seizure activity estimated using ECoG recordings in humans.

As a final illustration of the method described in this note, we estimated the excitatory gain parameter of the CMC for epileptic seizure activity using recordings from two patients with cortical dysplasia and refractory epilepsy. The ECoG data was collected retrospectively from the database at Clinical Neurophysiology at Great Ormond Street Hospital for Children NHS Foundation Trust Great Ormond Street, London, UK (data set 1) and at Karolinska University Hospital, Stockholm, Sweden (data set 2). Subdural recordings were made from a 32-contact and a 20-contact platinum array (Ad-Tech) placed over the lesion. Recordings were made

using Neuroscan and Nervus equipment, sampling at 1 kHz with a bandpass of 0.1–200 Hz, with an average reference. Seizure activity as seen in data set 1 is shown in figure 6. The seizure starts with low amplitude, high frequency activity that shows some evidence of spread and clear change in amplitude during the seizure. The seizure activity lasts for approximately 25 seconds, after which it abruptly terminates. Seizure activity as seen in data set 2 showed quick spreading between electrodes with duration of approximately 5 seconds. After the seizure, depressed low frequency activity was seen, i.e. post-ictal activity, figure 7. We used two seizures free of artefacts from each data set for modelling the averaged induced spectral activity. The time frequency response over each electrode was calculated using sequential 1000ms windows (which retained 95% of the total spectral power as estimated using a complex Gaussian wavelet).

[Figure 6]

[Figure 7]

The seizure activity in data set 1 showed increased spectral power at around 20 Hz that decreased to about 10 Hz towards the end of the seizure, figure 8. The data were inverted using the generative model described above. The eigenfunction in this case consisted of products of sine functions. This allowed modelling of non-isotropic diffusion and was not constrained to the rotationally symmetric dynamics used for simulating two dimensional dynamics above. The inversion of this model was performed using the same Bayesian belief updating scheme (see Appendix C), where the spatial fluctuations affected the excitatory gain parameter. The model also estimated parameters (without spatiotemporal dynamics) of intrinsic connectivity within the cortical column that were sampled from a white noise process. We allowed this random variation during Bayesian belief updating to accommodate unmodelled changes during the seizure activity.

[Figure 8]

The parameters inferred from these data were used to predict the spectral activity at each electrode. There was a good fit between the data and the predicted activity (explained variation > 0.85), figure 9.

[Figure 9]

Spatial dynamics controlling cortical excitability were inferred from the data, enabling excitatory gain to be estimated at each point within the cortical grid over time. There was an increase in this parameter in the regions to the right of the grid increasing to a maximum towards the end of the seizure and then quickly dissipating during termination of the seizure, figure 10.

In addition to the change in cortical excitability mediated by the spatiotemporal parameter, we also modelled fluctuations in an intrinsic connectivity parameter (the self-inhibition of superficial pyramidal cells: see Appendix A) at each source or electrode. These intrinsic parameters were allowed to vary randomly during the seizure; mimicking the variation in intrinsic variables expected in the brain – and accommodating unmodelled changes during seizure activity. There was a slight increase in variation of these parameters between the locations of the grid during seizure activity, as can be seen by the increase in variation around 20s.

[Figure 11]

An identical analysis was performed on the seizure recording from data set 2. Seizure activity was seen in several electrodes around 20 s. As seen in the raw data, there was a very fast spread between electrodes: see figure 12. Predicted responses – based on the estimated spatial dynamics of net cortical excitatory gain – showed good fits with the measured data (explained variation > 0.85); see figure 13. The spatial dynamics revealed an increase in excitatory gain during the seizure; however, the regions with increased activity were not confluent as in the previous case, and instead several individual foci were seen; see figure 14. The intrinsic parameters did not show any clear temporal variation during the seizure, though there was a short increase in variation during the termination of the seizure.

[Figure 12]

[Figure 13]

[Figure 14]

[Figure 15]

Discussion

This technical note provides a framework for analysing the spatiotemporal dynamics of epileptic seizure activity. We extended an inference scheme previously described for inference about the temporal structure of seizure activity using a field model to incorporate spatial dynamics (Cooray et al., 2015b). Including spatial processes models the spreading of epileptic seizure activity, which is one of the key physiological processes underlying a focal seizure. A deeper understanding of the spatial spread of focal seizures over the cortex could be used for curtailing the spread of a seizure; limiting its effect on the patient by either surgical or other procedures such as direct or induced electrical currents delivered by e.g. transcranial magnetic stimulation or deep brain stimulation (Engel, 1993, Rotenberg et al., 2008, Rossi et al., 2009).

The current framework for the analysis of seizure activity assumes that the temporal dynamics of cortical activity is several orders of magnitude faster than the dynamics of the spatiotemporal parameters controlling activity – and secondly that the spatial dynamics can be estimated using a finite set of eigenfunctions of the underlying partial differential equation. The second assumption was made for computational expediency. This assumption is only valid for relatively simple spatiotemporal dynamics (partial differential equations with analytical solutions) on simple representations of the cortical surface (such as a plane or spherical surface) (Evans, 2010). If any of these assumptions are violated, as in the case of realistic geometries obtained using MRI, the forward model would require re-formulation using numerical approximations; e.g., Finite element methods (Lui, 2012). Moreover, even if the assumptions are valid, the truncation of the analytic series of eigenfunctions might induce discontinuities at the boundaries. We will alleviate these issues by reformulating our scheme under a finite element framework using the approach described in Sengupta and Friston (2016). Although this will require extensive computational expenditure (in terms of high performance computing), it may be the only way forward; especially for patient specific MR-guided resection of the epileptogenic zone (CF, precision medicine). The real value of this work therefore lies in the potential to fit the parameters of spatiotemporal models of generative models to individual patients. This should allow one to understand individual differences that not only guide epileptogenic resections but also predict epilepsy surgery outcomes.

The first assumption that the temporal dynamics of the cortical columns is several orders of magnitude faster than the dynamics of the spatiotemporal parameters has support in experimental epileptology; as the slow spread of extracellular electrolytes, metabolites or oxygen concentration has been shown to affect seizure activity (Grafstein, 1956, Fetzinger and Ranck, 1970, Madison and Niedermeyer, 1970, Cornell-Bell et al., 1990, Finkbeiner, 1992, Ingram et al., 2014, Wei et al., 2014b, Ullah et al., 2015). The homeostasis of these electrolytes and metabolites is partly controlled by the glial system, where mainly astrocytes carefully adjust the concentration of extracellular factors. Several models have been proposed describing the interaction of glial and neuronal cells (Haydon and Carmignoto, 2006). Moreover, the capillary blood flow through the cortex may also affect extracellular concentrations of metabolites.

The spatiotemporal dynamics used in this note was a simple diffusion process. More realistic models would require precise models of glial-neural cell interaction, capillary blood flow and inhibitory neural cell dampening (Chander and Chakravarthy, 2012, Schevon et al., 2012, Jolivet et al., 2015). These modifications would require the use of numerical techniques for solving the spatiotemporal dynamics as describe above. This is again something we will consider in future studies.

The generative model presented in this note differs from the neural fields described by Amari, Wilson and Cowan as neural field models consider the interaction between points of a neural sheet (or a cortical region) due to structural (axonal) connections between neurons. These generative models are governed by integro-differential equations and the spatiotemporal dynamics are not restricted to slow time scales. This allows these neural models to generate a richer spectrum of behaviour than the (adiabatic diffusion) models used in this note. See Appendix D for more technical details regarding neural field and parameter field models. The cost of neural field models is there computational complexity and the difficulties in inferring parameters from the measured data. The complexity of integro-differential equations neural field models has been reduced partially, enabling them to be used in the DCM framework (Pinotsis et al., 2012). In this study we did not find it necessary to include integro-differential equations – as we were mainly interested in the slow spread of seizure activity, as opposed to the fast frequencies of seizure activity itself, i.e. our biological model was based on a diffusion model of extracellular factors, with a dynamics that was much slower than that of the cortical columns. A more general formulation of the problem of seizure spread would,

however, need to include axonal neuron-to-neuron interaction; resulting in integro-differential equations, whose parameters were themselves governed by diffusion dynamics.

In the numerical examples presented in this note, we used the CMC to represent cortical columns. This has been shown in several studies to give a suitable approximation of the human neocortex – retaining enough complexity to model the flow of information in predictive coding of sensory afferents but simple enough to allow for tractable numerical analysis for inference (Bastos et al., 2015). The CMC has also been used previously to model seizure activity, which sometimes includes complex multi-modular spectral peaks (Cooray et al., 2015a, Cooray et al., 2015b, Papadopoulou et al., 2015).

In dynamic causal modelling, it is essential to compare different generative models by comparing their evidence; usually approximated by the variational free energy optimised during model inversion. The total free energy of the filtering scheme can be estimated as the sum of the free energies for each window (Stephan et al., 2010, Cooray et al., 2015b). This could include generative models with different spatiotemporal dynamics of the spatially varying parameter (i.e. partial differential equations). If both sets of generative models have the same eigenfunction, Bayesian model comparison would proceed using free energy in the usual way. This comparison would, however, require nuancing, if any of the models had a different eigenfunction basis. In this case, the method for inference would need to be modified where a more involved numerical approximation would be required (cf. Sengupta and Friston 2016). In the examples presented above, evaluating model evidence was trivial; as we projected our inference onto an eigenfunction subspace spanned by a small finite number of eigenfunctions. However, the use of standard inversion of partial differential equations will increase the complexity of the inference requiring greater processing power. To achieve simple numerical analysis of this problem, spatiotemporal dynamics with known eigenfunctions are required. The simple geometries like the plane (as used in this study) or spherical regions often have known eigenfunctions (Evans, 2010), which is why they were utilised here.

The method we described assumed the invasive electrodes to be sampling a cortex modelled as a plane at specific points. This method also requires assumptions about how seizure activity spreads along the surface, which can be evaluated and tested using Bayesian model comparison as described above. By including spatiotemporal dynamics, we can make inferences about the activity of regions outside the arrays of sensors. This would not be

possible if we treated each sensor as a node connected in a network. This is of importance in the field of epileptology, as one of the main goals is disclosing the origin of seizures, which might not always be sampled directly by any sensor (Engel, 1993). Relocating sensors surgically after analysis is often not possible, due to the increased risks for patients being investigated.

Furthermore, the models proposed here also give a unique opportunity to model the effects of different interventions: like virtual patients, they can be used to evaluate the effects of removing a specific node or changing specific connection strengths. Spatiotemporal models can also generate dynamics that are qualitatively different from pure neural mass models (Baier et al., 2012, Goodfellow et al., 2012) suggesting that these models may have the potential to explain mechanistically observed features that are not easily reproduced with pure neural masses, such as spontaneous seizure on- and offset.

In conclusion, we present a straightforward way of extending an established Bayesian belief update or filtering scheme to include the spatial spread of seizure activity. This requires several (plausible) assumptions regarding the behaviour of cortical columns, the geometry of the cortex and a separation of time scales of fast neuronal activity and slower fluctuations in cortical gain. We suggest that these assumptions have some experimental evidence but that the method can be modified if these assumptions are shown to be invalid or too inaccurate in the future. In particular, by comparing different spatiotemporal models (e.g. diffusion versus reaction diffusion models), using their model evidence, the above framework could be used to address important questions about how seizure activity spreads in patients.

Appendix

A Canonical Microcircuit

The cortical columns described in this note were modelled using a neural mass model generating electrographic seizure activity. The canonical cortical microcircuit (CMC) is comprised of four subpopulations of neurons corresponding to superficial and deep pyramidal, excitatory, and inhibitory cells (Moran et al., 2013, Bastos et al., 2015). These cell populations are connected using ten inhibitory and excitatory connections. Afferent connections drove the excitatory granular cells and efferent connections derive from the superficial pyramidal cells.

[Figure A1]

The equations governing the neural mass were given by,

$$\ddot{x}_e + \frac{2\dot{x}_e}{T_e} + \frac{x_e}{T_e^2} = -g_1s(x_e) - g_3s(x_i) - g_2s(x_{sp}) \quad A1$$

$$\ddot{x}_i + \frac{2\dot{x}_i}{T_i} + \frac{x_i}{T_i^2} = \theta_{sp}g_5s(x_e) + \theta_{sp}g_6s(x_{dp}) - g_4s(x_i) \quad A2$$

$$\ddot{x}_{sp} + \frac{2\dot{x}_{sp}}{T_{sp}} + \frac{x_{sp}}{T_{sp}^2} = \theta_{sp}g_8s(x_e) - g_7s(x_{sp}) \quad A3$$

$$\ddot{x}_{dp} + \frac{2\dot{x}_{dp}}{T_{dp}} + \frac{x_{dp}}{T_{dp}^2} = -g_{10}s(x_{dp}) - g_9s(x_i) \quad A4$$

θ_{sp} is the parameter with spatiotemporal dynamics described in this note. Parameter g_7 was sampled from a Gaussian distribution during the Bayesian filtering process as describe above. All other parameters were kept constant during the inversion. These constant values are given in table 1.

[Table 1]

B Solution of parameter field equations

Heat equation with time dependent boundary conditions in 1 spatial dimension; the formulas can be easily re-derived for the multidimensional case.

$u(x, t)$ = parameter with spatiotemporal variation

α = diffusion coefficient

$\varphi_{1/0}(t)$ = boundary condition (time dependent)

$f(x)$ = initial condition of parameter

L = length of one dimensional domain over which u varies

$\omega(x)$ = time independent particular solution

$v(x, t)$ = homogenous solution to diffusion equation

$S(x, t)$ = auxillary variable

$$\begin{cases} u_t = \alpha^2 u_{xx} \\ u(0, t) = \varphi_0, \quad u(L, t) = \varphi_1 \\ u(x, 0) = f(x) \end{cases} \quad B1$$

$$\omega = \varphi_0 + \frac{x}{L}(\varphi_1 - \varphi_0) \quad B2$$

$$u = \omega + v \quad B3$$

$$u_t = \omega_t + v_t = \alpha^2 v_{xx} \quad B4$$

$$\begin{cases} v_t = \alpha^2 v_{xx} - \omega_t \\ v(0, t) = v(L, t) = 0 \\ v(x, 0) = f(x) - \omega(x, 0) \end{cases} \quad B5$$

$$S(x, t) = -\frac{d\omega}{dt} \quad B6$$

The solution to the diffusion equation (B1) above will be separated into time and space dependent functions; i.e separation of variables. The full solution can be written as an infinite series of eigenfunctions (space dependent functions), together with their time dependent variation. The eigenfunctions of the diffusion equation will all satisfy an equivalent ordinary differential equation. Thus the solutions to the ordinary differential equation will give the eigenfunctions or eigenvectors representing its solutions and their eigenvalues. These inform the rate of decay of the eigenfunctions, when seen as solutions to the original diffusion equation. For the one dimensional diffusion equation with Dirichlet boundary conditions (zero along boundaries) the eigenfunctions can be written as sine functions. For the two

dimensional case with rotational symmetry a linear combination of first and second order Bessel functions can be used.

λ_n = eigenvalue of ordinary differential equation

$S_n(t)$ = coefficient of the eigenfunction $\sin \lambda_n x$ in the eigenfunction expansion of the auxillary variable $S(x, t)$

$v_n(t)$ = coefficient of the eigenfunction $\sin \lambda_n x$ in the eigenfunction expansion of $v(x, t)$

c_n = coefficient of the eigenfunction $\sin \lambda_n x$ in the eigenfunction expansion of the intial condition of $v(x, t)$, i.e. $v(x, 0)$

$$S(x, t) = \sum_{n=1}^{\infty} S_n(t) \sin \lambda_n x \quad B7$$

$$S_n(t) = -\frac{2}{L} \int_0^L \frac{d\omega}{dt} \sin \lambda_n x dx \quad B8$$

$$\lambda_n = \frac{n\pi}{L} \quad B9$$

$$v(x, t) = \sum_{n=1}^{\infty} v_n(t) \sin \lambda_n x \quad B10$$

$$v(x, 0) = \sum_{n=1}^{\infty} c_n \sin \lambda_n x \quad B11$$

$$c_n = \frac{2}{L} \int_0^L (f(x) - \omega(x, 0)) \sin \lambda_n x dx \quad B12$$

$$u(x, t) = \omega(x, t) + \sum_{n=1}^{\infty} \left(\int_0^t S_n(\tau) \exp(-\alpha^2 \lambda_n^2 \tau) d\tau + c_n \right) \exp(-\alpha^2 \lambda_n^2 t) \sin \lambda_n x \quad B13$$

C Bayesian belief updating

The following equations give the Bayesian belief updating of the parameters as data is inverted sequentially across the windowed data, y_i , see Cooray for more details (Cooray et al., 2016). The priors of the n eigenfunction coefficients of parameter θ_{sp} in each window is given by the following:

μ_i = posterior mean vector of θ_{sp} in i^{th} window i.e. $(c_1, c_2, \dots, c_n)_i$

$\vec{\lambda}$ = eigenvalue vector of eigenfunctions, i.e. $(\lambda_1, \lambda_2, \dots, \lambda_n)$

Δ = time interval between windows, i.e. 1 s.

Q_i = posterior covariance matrix of θ_{sp} in i^{th} window

\mathcal{R} = volatility covariance matrix of θ_{sp}

$p(\theta_{sp} | y_i, \dots, y_1)$ = prior probability density of θ_{sp} in $i+1^{\text{th}}$ window.

$$p(\theta_{sp} | y_i, \dots, y_1) = \mathcal{N}(\mu_i e^{-\vec{\lambda}\Delta}, Q_i + \mathcal{R})$$

Using variational bayes this prior probability distribution is updated with the data of window $i+1$. The self-inhibition of the superficial pyramidal cells, g_7 (Eq. A3), is also estimated in each window though the prior of this parameter is sampled from a constant normal distribution, i.e. priors are not updated.

D Difference between a neural field model and a parameter field model

Neural field

$u(x, t)$ = neural field representing activity of a population of neurons at location x at time t

$w(y)$ = the strength of connections between neurons separated by a distance y

$f(u)$ = firing rate function

$$u_t(x, t) = -u + \int_{-\infty}^{\infty} dy w(y) f(u(x - y, t)) \quad C1$$

Parameter field

$u(x, t)$ = neural field representing activity of a population of neurons at location x at time t

$f(u)$ = firing rate function

$\theta(x, t)$ = parameter field

k = rate coefficient of neural mass

α = diffusion coefficient

$$\begin{cases} u_{tt}(x, t) - 2ku_t(x, t) - k^2u(x, t) = f(u(x, t), \theta(x, t)) \\ \theta_t = \alpha^2\theta_{xx} \end{cases} \quad C2$$

Note that the spatial variation of the neural field in the case of *C1* is due to the time independent variable w . As this term is convolved over space with the firing rate it is not possible to separate the spatial and the temporal dynamics. In the case of *C2* though it is possible to have only a slowly diffusing parameter (diffusion rate dependent on α , second row) which interacts as though it is a constant with the dynamics of the faster neural mass (rate dependent on k , first row).

References

- Amari S (1977) Dynamics of pattern formation in lateral-inhibition type neural fields. *Biol Cybern* 27:77-87.
- Asano E, Juhasz C, Shah A, Muzik O, Chugani DC, Shah J, Sood S, Chugani HT (2005) Origin and propagation of epileptic spasms delineated on electrocorticography. *Epilepsia* 46:1086-1097.
- Baier G, Goodfellow M, Taylor PN, Wang Y, Garry DJ (2012) The importance of modeling epileptic seizure dynamics as spatio-temporal patterns. *Frontiers in physiology* 3:281.
- Bastos AM, Litvak V, Moran R, Bosman CA, Fries P, Friston KJ (2015) A DCM study of spectral asymmetries in feedforward and feedback connections between visual areas V1 and V4 in the monkey. *NeuroImage* 108:460-475.
- Benjamin O, Fitzgerald TH, Ashwin P, Tsaneva-Atanasova K, Chowdhury F, Richardson MP, Terry JR (2012) A phenomenological model of seizure initiation suggests network structure may explain seizure frequency in idiopathic generalised epilepsy. *J Math Neurosci* 2:1.
- Blenkinsop A, Valentin A, Richardson MP, Terry JR (2012) The dynamic evolution of focal-onset epilepsies--combining theoretical and clinical observations. *Eur J Neurosci* 36:2188-2200.
- Breakspear M, Roberts JA, Terry JR, Rodrigues S, Mahant N, Robinson PA (2006) A unifying explanation of primary generalized seizures through nonlinear brain modeling and bifurcation analysis. *Cereb Cortex* 16:1296-1313.
- Chander BS, Chakravarthy VS (2012) A computational model of neuro-glio-vascular loop interactions. *PLoS one* 7:e48802.
- Coombes S (2005) Waves, bumps, and patterns in neural field theories. *Biol Cybern* 93:91-108.
- Coombes S, Venkov NA, Shiao L, Bojak I, Liley DT, Laing CR (2007) Modeling electrocortical activity through improved local approximations of integral neural field equations. *Phys Rev E Stat Nonlin Soft Matter Phys* 76:051901.
- Cooray GK, Sengupta B, Douglas P, Englund M, Wickstrom R, Friston K (2015a) Characterising seizures in anti-NMDA-receptor encephalitis with dynamic causal modelling. *NeuroImage* 118:508-519.
- Cooray GK, Sengupta B, Douglas PK, Friston K (2015b) Dynamic causal modelling of electrographic seizure activity using Bayesian belief updating. *NeuroImage*.
- Cooray GK, Sengupta B, Douglas PK, Friston K (2016) Dynamic causal modelling of electrographic seizure activity using Bayesian belief updating. *NeuroImage* 125:1142-1154.
- Cornell-Bell AH, Finkbeiner SM, Cooper MS, Smith SJ (1990) Glutamate induces calcium waves in cultured astrocytes: long-range glial signaling. *Science* 247:470-473.
- Daunizeau J, Kiebel SJ, Friston KJ (2009) Dynamic causal modelling of distributed electromagnetic responses. *NeuroImage* 47:590-601.
- David O, Guillemain I, Sallet S, Reyt S, Deransart C, Segebarth C, Depaulis A (2008) Identifying neural drivers with functional MRI: an electrophysiological validation. *PLoS Biol* 6:2683-2697.
- Deco G, Jirsa VK, Robinson PA, Breakspear M, Friston K (2008) The dynamic brain: from spiking neurons to neural masses and cortical fields. *PLoS computational biology* 4:e1000092.
- Engel J (1993) *Surgical treatment of the epilepsies*. New York: Raven Press.
- Engel J, Jr. (1995) Inhibitory mechanisms of epileptic seizure generation. *Adv Neurol* 67:157-171.
- Evans CE (2010) *Partial Differential Equations: American Mathematical Society*.
- Fertziger AP, Ranck JB, Jr. (1970) Potassium accumulation in interstitial space during epileptiform seizures. *Exp Neurol* 26:571-585.
- Finkbeiner S (1992) Calcium waves in astrocytes-filling in the gaps. *Neuron* 8:1101-1108.
- Freestone DR, Karoly PJ, Netic D, Aram P, Cook MJ, Grayden DB (2014) Estimation of effective connectivity via data-driven neural modeling. *Front Neurosci* 8:383.

- Friston KJ, Bastos A, Litvak V, Stephan KE, Fries P, Moran RJ (2012) DCM for complex-valued data: cross-spectra, coherence and phase-delays. *NeuroImage* 59:439-455.
- Frohlich F, Sejnowski TJ, Bazhenov M (2010) Network bistability mediates spontaneous transitions between normal and pathological brain states. *The Journal of neuroscience : the official journal of the Society for Neuroscience* 30:10734-10743.
- Golomb D, Amitai Y (1997) Propagating neuronal discharges in neocortical slices: computational and experimental study. *Journal of neurophysiology* 78:1199-1211.
- Goodfellow M, Schindler K, Baier G (2012) Self-organised transients in a neural mass model of epileptogenic tissue dynamics. *NeuroImage* 59:2644-2660.
- Grafstein B (1956) Mechanism of spreading cortical depression. *Journal of neurophysiology* 19:154-171.
- Grimbert F, Faugeras O (2006) Bifurcation analysis of Jansen's neural mass model. *Neural Comput* 18:3052-3068.
- Haydon PG, Carmignoto G (2006) Astrocyte control of synaptic transmission and neurovascular coupling. *Physiological reviews* 86:1009-1031.
- Ingram J, Zhang C, Cressman JR, Hazra A, Wei Y, Koo YE, Ziburkus J, Kopelman R, Xu J, Schiff SJ (2014) Oxygen and seizure dynamics: I. Experiments. *Journal of neurophysiology* 112:205-212.
- Jansen BH, Rit VG (1995) Electroencephalogram and visual evoked potential generation in a mathematical model of coupled cortical columns. *Biol Cybern* 73:357-366.
- Jirsa VK, Haken H (1996) Field Theory of Electromagnetic Brain Activity. *Physical review letters* 77:960-963.
- Jirsa VK, Kelso JA (2000) Spatiotemporal pattern formation in neural systems with heterogeneous connection topologies. *Phys Rev E Stat Phys Plasmas Fluids Relat Interdiscip Topics* 62:8462-8465.
- Jirsa VK, Stacey WC, Quilichini PP, Ivanov AI, Bernard C (2014) On the nature of seizure dynamics. *Brain* 137:2210-2230.
- Jolivet R, Coggan JS, Allaman I, Magistretti PJ (2015) Multi-timescale modeling of activity-dependent metabolic coupling in the neuron-glia-vasculature ensemble. *PLoS computational biology* 11:e1004036.
- Kager H, Wadman WJ, Somjen GG (2000) Simulated seizures and spreading depression in a neuron model incorporating interstitial space and ion concentrations. *Journal of neurophysiology* 84:495-512.
- Liley DT, Cadusch PJ, Dafilis MP (2002) A spatially continuous mean field theory of electrocortical activity. *Network* 13:67-113.
- Loewenstein Y, Sompolinsky H (2003) Temporal integration by calcium dynamics in a model neuron. *Nat Neurosci* 6:961-967.
- Lopes da Silva FH, Blanes W, Kalitzin SN, Parra J, Suffczynski P, Velis DN (2003) Dynamical diseases of brain systems: different routes to epileptic seizures. *IEEE Trans Biomed Eng* 50:540-548.
- Lui S, H. (2012) *Numerical Analysis of Partial Differential Equations*. Hoboken, New Jersey: Wiley-Blackwell.
- Madison D, Niedermeyer E (1970) Epileptic seizures resulting from acute cerebral anoxia. *Journal of neurology, neurosurgery, and psychiatry* 33:381-386.
- Moran R, Pinotsis DA, Friston K (2013) Neural masses and fields in dynamic causal modeling. *Front Comput Neurosci* 7:57.
- Moran RJ, Jung F, Kumagai T, Endepols H, Graf R, Dolan RJ, Friston KJ, Stephan KE, Tittgemeyer M (2011a) Dynamic causal models and physiological inference: a validation study using isoflurane anaesthesia in rodents. *PloS one* 6:e22790.
- Moran RJ, Mallet N, Litvak V, Dolan RJ, Magill PJ, Friston KJ, Brown P (2011b) Alterations in brain connectivity underlying beta oscillations in Parkinsonism. *PLoS computational biology* 7:e1002124.
- Moran RJ, Stephan KE, Dolan RJ, Friston KJ (2011c) Consistent spectral predictors for dynamic causal models of steady-state responses. *NeuroImage* 55:1694-1708.

- Nadkarni S, Jung P (2003) Spontaneous oscillations of dressed neurons: a new mechanism for epilepsy? *Physical review letters* 91:268101.
- Nevado-Holgado AJ, Marten F, Richardson MP, Terry JR (2012) Characterising the dynamics of EEG waveforms as the path through parameter space of a neural mass model: application to epilepsy seizure evolution. *NeuroImage* 59:2374-2392.
- Papadopoulou M, Leite M, van Mierlo P, Vonck K, Lemieux L, Friston K, Marinazzo D (2015) Tracking slow modulations in synaptic gain using dynamic causal modelling: validation in epilepsy. *NeuroImage* 107:117-126.
- Pinotsis DA, Moran RJ, Friston KJ (2012) Dynamic causal modeling with neural fields. *NeuroImage* 59:1261-1274.
- Rennie CJ, Wright JJ, Robinson PA (2000) Mechanisms of cortical electrical activity and emergence of gamma rhythm. *J Theor Biol* 205:17-35.
- Risken H, Frank T (1996) *The Fokker-Planck Equation*: Springer.
- Robinson PA (2006) Patchy propagators, brain dynamics, and the generation of spatially structured gamma oscillations. *Phys Rev E Stat Nonlin Soft Matter Phys* 73:041904.
- Robinson PA, Rennie CJ, Rowe DL (2002) Dynamics of large-scale brain activity in normal arousal states and epileptic seizures. *Phys Rev E Stat Nonlin Soft Matter Phys* 65:041924.
- Rossi S, Hallett M, Rossini PM, Pascual-Leone A, Safety of TMS (2009) Safety, ethical considerations, and application guidelines for the use of transcranial magnetic stimulation in clinical practice and research. *Clinical neurophysiology : official journal of the International Federation of Clinical Neurophysiology* 120:2008-2039.
- Rotenberg A, Muller P, Birnbaum D, Harrington M, Riviello JJ, Pascual-Leone A, Jensen FE (2008) Seizure suppression by EEG-guided repetitive transcranial magnetic stimulation in the rat. *Clinical neurophysiology : official journal of the International Federation of Clinical Neurophysiology* 119:2697-2702.
- Rowe DL, Robinson PA, Rennie CJ (2004) Estimation of neurophysiological parameters from the waking EEG using a biophysical model of brain dynamics. *J Theor Biol* 231:413-433.
- Sarkka S, Solin A, Nummenmaa A, Vehtari A, Auranen T, Vanni S, Lin FH (2012) Dynamic retrospective filtering of physiological noise in BOLD fMRI: DRIFTER. *NeuroImage* 60:1517-1527.
- Schevon CA, Weiss SA, McKhann G, Jr., Goodman RR, Yuste R, Emerson RG, Trevelyan AJ (2012) Evidence of an inhibitory restraint of seizure activity in humans. *Nature communications* 3:1060.
- Schiff SJ, Sauer T (2008) Kalman filter control of a model of spatiotemporal cortical dynamics. *J Neural Eng* 5:1-8.
- Solin A (2012) Hilbert space methods in infinite dimensional kalman filtering. In: Department of Biomedical Engineering and Computational Science, Alto University, vol. Masters thesis, p 64 Espoo: Alto University.
- Stephan KE, Harrison LM, Kiebel SJ, David O, Penny WD, Friston KJ (2007) Dynamic causal models of neural system dynamics: current state and future extensions. *J Biosci* 32:129-144.
- Stephan KE, Penny WD, Moran RJ, den Ouden HE, Daunizeau J, Friston KJ (2010) Ten simple rules for dynamic causal modeling. *NeuroImage* 49:3099-3109.
- Traub RD, Duncan R, Russell AJ, Baldeweg T, Tu Y, Cunningham MO, Whittington MA (2010) Spatiotemporal patterns of electrocorticographic very fast oscillations (> 80 Hz) consistent with a network model based on electrical coupling between principal neurons. *Epilepsia* 51:1587-1597.
- Ullah G, Cressman JR, Jr., Barreto E, Schiff SJ (2009) The influence of sodium and potassium dynamics on excitability, seizures, and the stability of persistent states. II. Network and glial dynamics. *J Comput Neurosci* 26:171-183.
- Ullah G, Schiff SJ (2010) Assimilating seizure dynamics. *PLoS computational biology* 6:e1000776.
- Ullah G, Wei Y, Dahlem MA, Wechselberger M, Schiff SJ (2015) The Role of Cell Volume in the Dynamics of Seizure, Spreading Depression, and Anoxic Depolarization. *PLoS computational biology* 11:e1004414.

- Wei Y, Ullah G, Ingram J, Schiff SJ (2014a) Oxygen and seizure dynamics: II. Computational modeling. *Journal of neurophysiology* 112:213-223.
- Wei Y, Ullah G, Schiff SJ (2014b) Unification of neuronal spikes, seizures, and spreading depression. *The Journal of neuroscience : the official journal of the Society for Neuroscience* 34:11733-11743.
- Wendling F, Hernandez A, Bellanger JJ, Chauvel P, Bartolomei F (2005) Interictal to ictal transition in human temporal lobe epilepsy: insights from a computational model of intracerebral EEG. *J Clin Neurophysiol* 22:343-356.
- Wilson HR, Cowan JD (1972) Excitatory and inhibitory interactions in localized populations of model neurons. *Biophys J* 12:1-24.
- Wilson HR, Cowan JD (1973) A mathematical theory of the functional dynamics of cortical and thalamic nervous tissue. *Kybernetik* 13:55-80.
- Vitikainen AM, Salli E, Lioumis P, Makela JP, Metsahonkala L (2013) Applicability of nTMS in locating the motor cortical representation areas in patients with epilepsy. *Acta Neurochir (Wien)* 155:507-518.

Figure legends

Figure 1A) Space time plot of the spatiotemporal dynamics of the parameter (θ_{sp}). Note that the values along the abscissa show the variation of θ_{sp} over time at the origin. B) The inferred variation in θ_{sp} . Note that there is a significant error along the abscissa, which is explained by the fact that the three eigenfunctions used for inference were zero along the abscissa. However, increasing the number of eigenfunctions from three would reduce the total error between the estimated and actual drift.

Figure 2. Top left shows the time frequency plot of seizure activity measured at electrode 1. Note the increase in wideband activity just before 20 s, which indicates the simulated seizure activity. Middle left shows the same for electrode 2. Bottom left for electrode 3, top right for electrode 4 and middle right for electrode 5. Bottom right shows the simulated variations for the excitatory parameter (θ_{sp}) at the five electrodes.

Figure 3. The spectral activity at the electrode locations of the grid is shown in time frequency plots, the x and y axis demarcating the grid is shown outside the time-frequency plots. The focus of the seizure activity is placed slightly beyond the top left corner of the grid. Note the increase in amplitude but also the decrease in onset latency of seizure activity for electrodes placed closer to the focus, compared with electrodes placed at a distance.

Figure 4. The spectral activity predicted from the dynamics of the spatial parameter inferred from the simulated data in the previous figure, the x and y axis demarcating the grid is shown outside the time frequency plots. Note the similarity of this estimated activity to simulated activity shown in figure 3 (explained variation > 0.99).

Figure 5. A) Space time plot of the spatiotemporal dynamics of the varying parameter (θ_{sp}). Note that the values along the abscissa show the prescribed variation of θ_{sp} over time at the origin. B) Inferred variation in θ_{sp} . Note that there is a good overall fit of the estimated fluctuations to the true (simulated) fluctuations (explained variation > 0.95). There is oscillatory activity in the estimated fluctuations to the left of the graph, which reduces the fit; however, by including more eigenfunctions (7 were used in the present inversion) on which the inference is estimated it is possible to reduce the total error between estimation and the actual drift.

Figure 6. Seizure activity recorded in data set 1 an ECoG grid. The seizure starts with low amplitude high frequency activity that spreads over several electrodes, increases in amplitude and decreases in frequency. The seizure terminates relatively fast and is followed by a short post-ictal period.

Figure 7. Seizure activity recorded in data set 2 using an ECoG grid. The seizure starts with low amplitude. High frequency activity and spreads very quickly over the electrode grid. Seizure activity increases in amplitude and decreases in frequency. The seizure terminates relatively fast and is followed by a short post-ictal period.

Figure 8. Time frequency plots of seizure activity (data set 1) over grid electrodes. The seizure activity showed increased spectral power at around 20 Hz which decreased to about 10 Hz toward the end of the seizure

Figure 9. The estimated parameters were used to estimate the spectral activity (data set 1) at each electrode. There was a good fit between the data and the predicted activity (explained variation > 0.85).

Figure 10. Spatiotemporal dynamics of net excitatory gain shown in the region of the cortical grid (data set 1). “Snapshots” are shown each 2.5 seconds. Note that there was an increase in excitatory gain towards the end of the seizure (a) with a quick dissipation during termination of the seizure (b).

Figure 11. The spatial variation in intrinsic connectivity (data set 1) was governed by parameter θ_{sp} (which itself was governed by spatial and temporal dynamics i.e., a partial differential equation) and parameter θ_i that was sampled repeatedly for each time window for each sensor position from a Gaussian distribution. The 32 samples (from the 32 electrodes) of θ_i for each time window is plotted over time where the mean is plotted in red and the two standard deviation interval with blue. These estimates suggest an increase in the variability of intrinsic connectivity over cortical locations, during the seizure indicating presence of unmodelled processes.

Figure 12. Time frequency plots of seizure activity (data set 2) over grid electrodes. The seizure activity showed increased spectral power at around 20 s with broadband activity over several electrodes in the grid. Immediately after the seizure, there was an attenuation of electrical activity that can be easily identified in the time frequency plots around 30s. Four electrodes were corrupted with artefactual noise for analysis and have been left out blank.

Figure 13. The estimated parameters were used to predict the spectral activity (data set 2) at each electrode. There was a good fit between the data and the predicted activity (explained variation > 0.85).

Figure 14. Spatiotemporal dynamics of excitatory gain shown in the region of the cortical grid (data set 2). “Snapshots” are shown each 2.5 seconds. Note that there was an increase in excitatory gain towards the end of the seizure (a) with a rapid dissipation at the termination of the seizure (b).

Figure 15. The spatial variation in intrinsic connectivity (cortical excitability, data set 2) was governed by parameter θ_{sp} (which itself was governed by spatial and temporal dynamics, partial differential equation) and parameters θ_i that were sampled repeatedly for each time window – for each sensor position – from a Gaussian distribution. The 16 samples (from the 16 electrodes) of θ_i for each time window is plotted over time where the mean is plotted in red and the two standard deviation interval with blue. These results show an increase in the variation over electrodes during the termination of the seizure indicating presence of unmodelled processes.

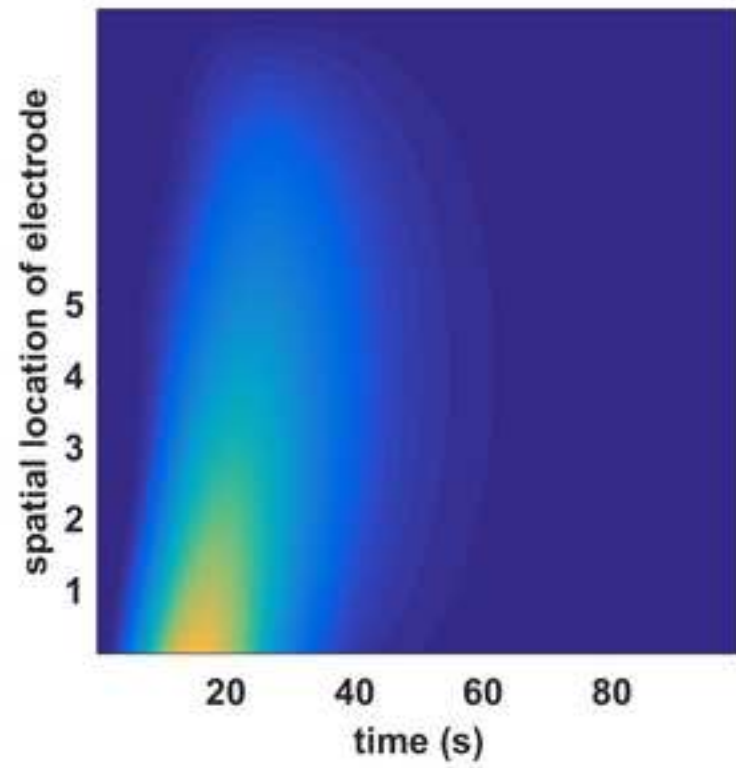
Figure A1. The canonical microcircuit (CMC) is comprised of four subpopulations of neurons corresponding to superficial and deep pyramidal, excitatory, and inhibitory cells. The excitatory gain parameter adjusts the strength of the excitatory connections shown in red. The other seven connections between the populations are not illustrated in the figure for clarity.

Table 1. Constant parameters of the Dynamic Causal Modelling. The endogenous spectral input describes constants used to define the input to the cortical columns which were assumed to be constant during the inversion (Cooray et al., 2015b).

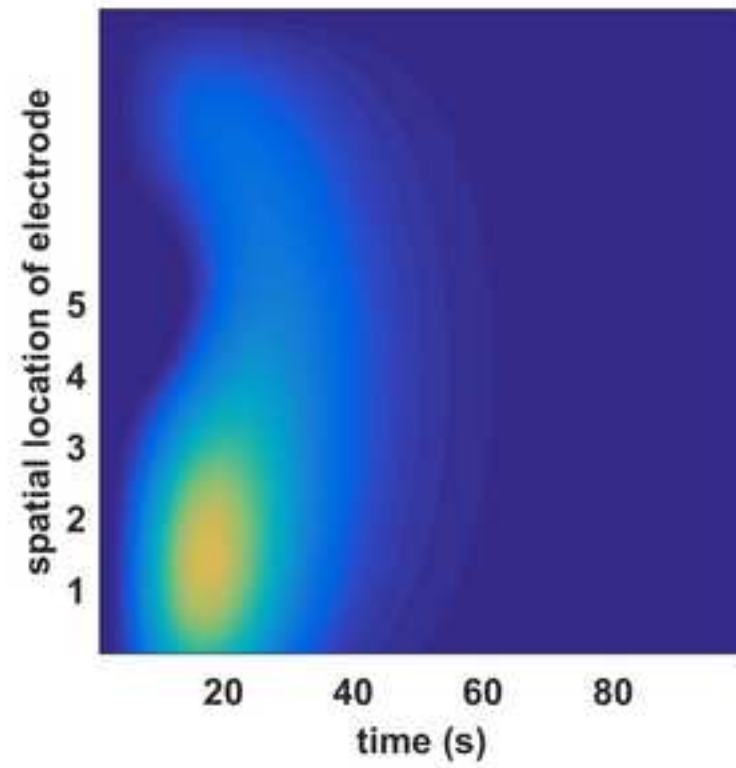
Parameters estimated		
Constant parameters	Notation	Constant value
Time constants (Hz)	$T_i, i=e,sp,i,dp$	$[0.25 \ 0.17 \ 0.08 \ 0.07]*1000$
Connectivity constants (Hz)	$g_i, i=1,2,10$	$[0.8, \dots, 0.2]*1000$
Slope of sigmoid function	Γ	0.67
Time delay for connections (ms)	D	1
<i>Connectivity parameters</i>		
Inhibitory (Hz)	$g_3(t)$	1.6*1000
Inhibitory (Hz)	$g_4(t)$	0.8*1000
Inhibitory (Hz)	$g_9(t)$	0.4*1000
Excitatory (Hz)	$g_5(t)$	0.8*1000
Excitatory (Hz)	$g_6(t)$	0.4*1000
Excitatory (Hz)	$g_8(t)$	0.8*1000
<i>Endogenous spectral input</i>		
Amplitude of spectral density of input	$a_1(t)$	1
Power law exponent of spectral density of input	$a_2(t)$	1
Amplitude of spectral density of measurement noise	$b_1(t)$	1
Power law exponent of spectral density of measurement noise	$b_1(t)$	1
Spectral innovation of input	$d_i(t), i=1, \dots, 8$	1

9. Figure 1
[Click here to download high resolution image](#)

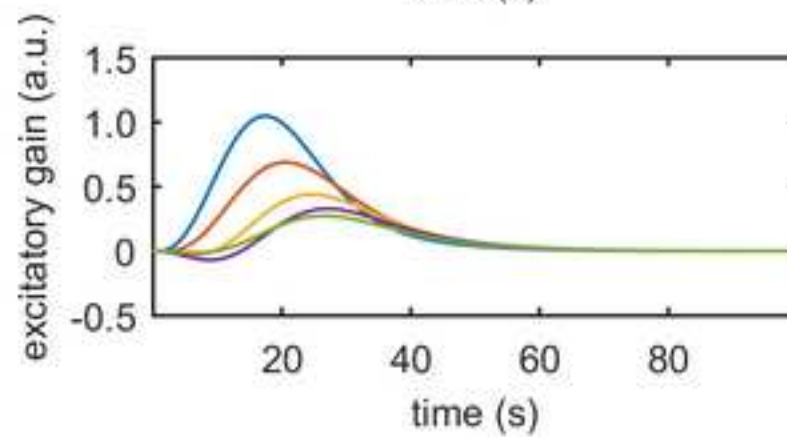
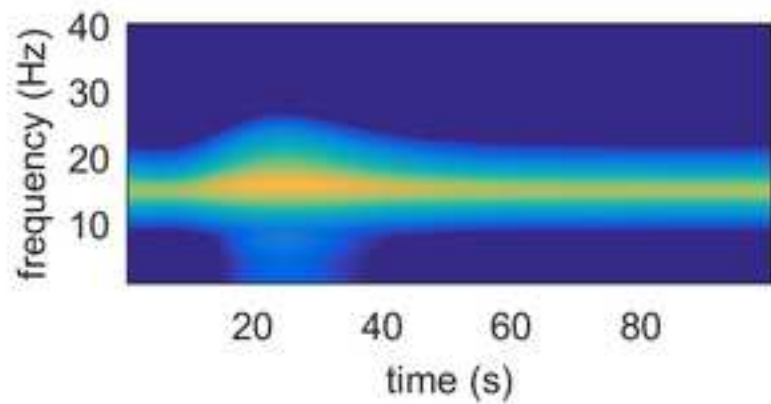
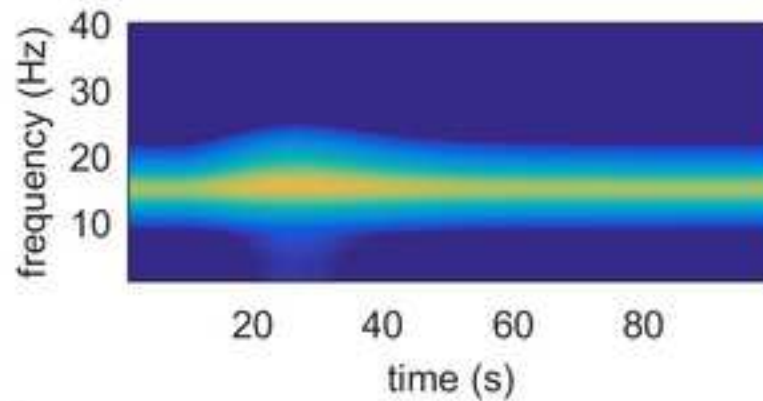
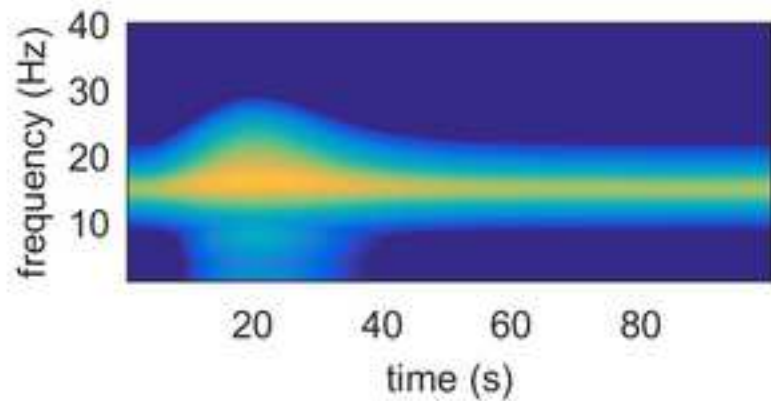
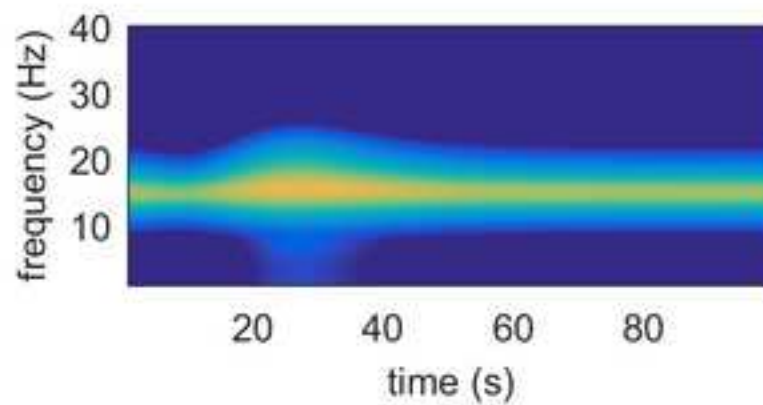
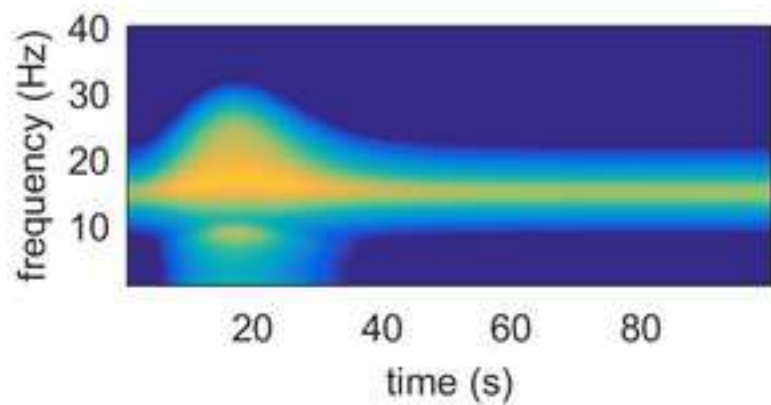
A



B

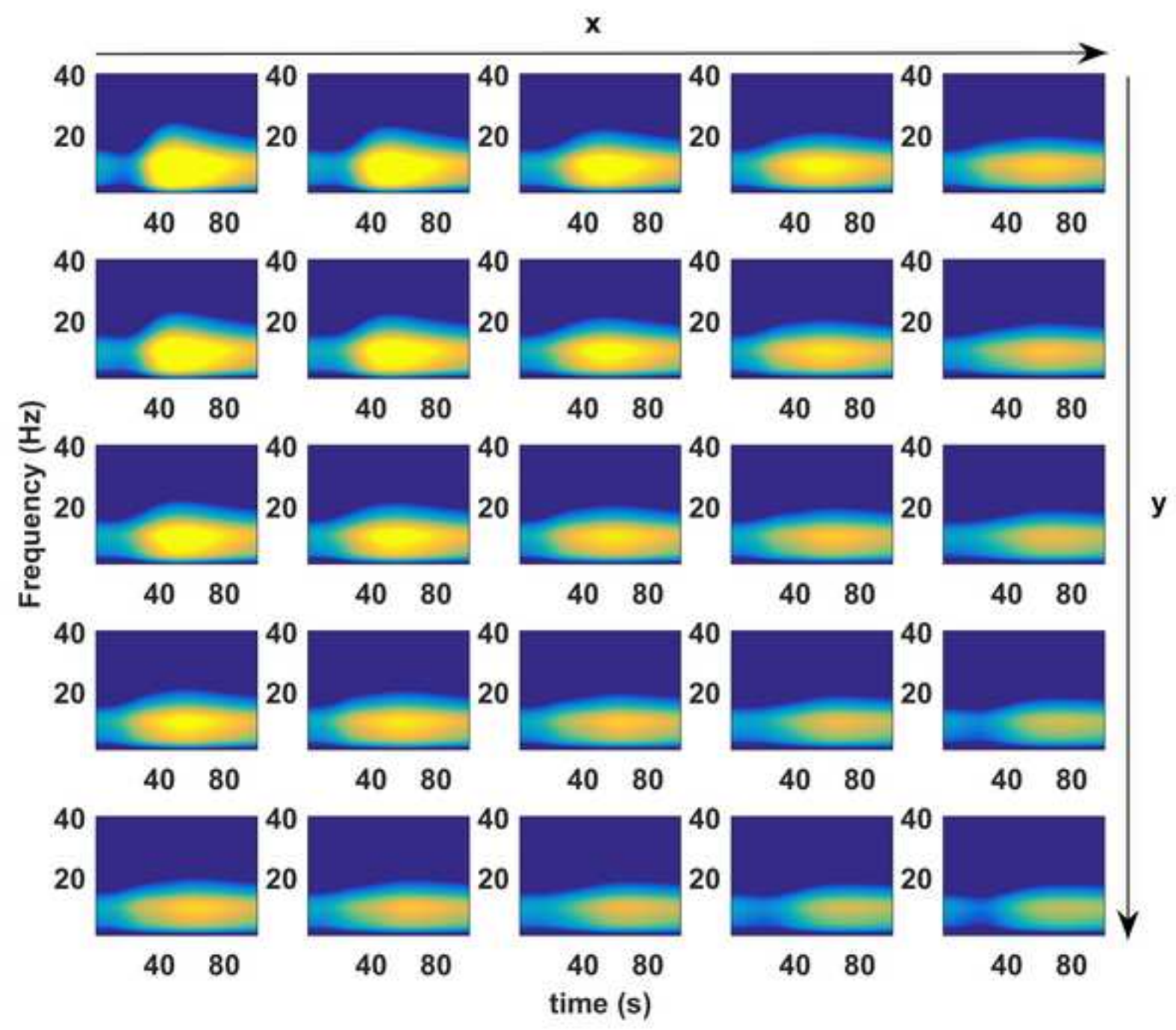


9. Figure 2
[Click here to download high resolution image](#)

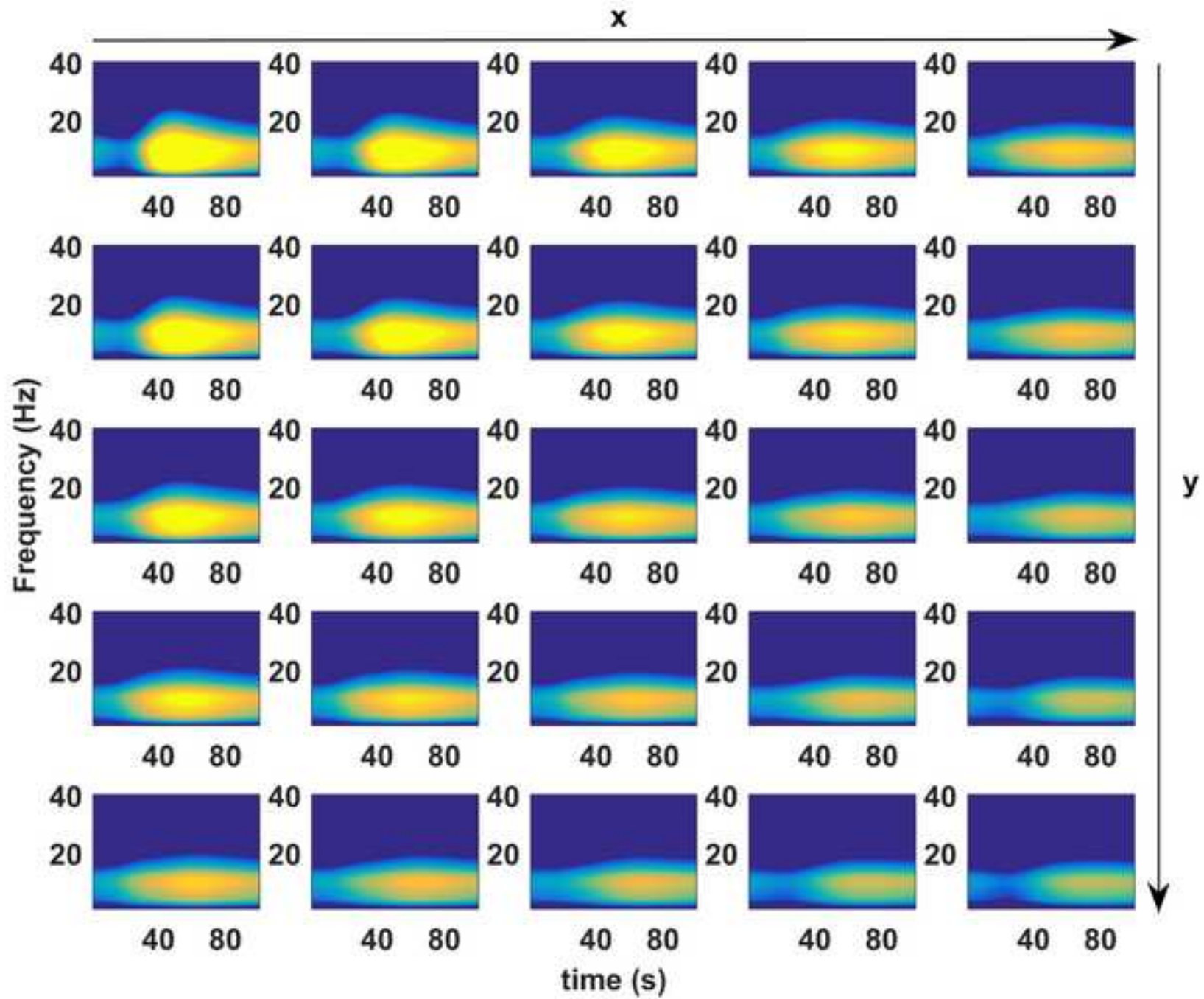


9. Figure 3

[Click here to download high resolution image](#)

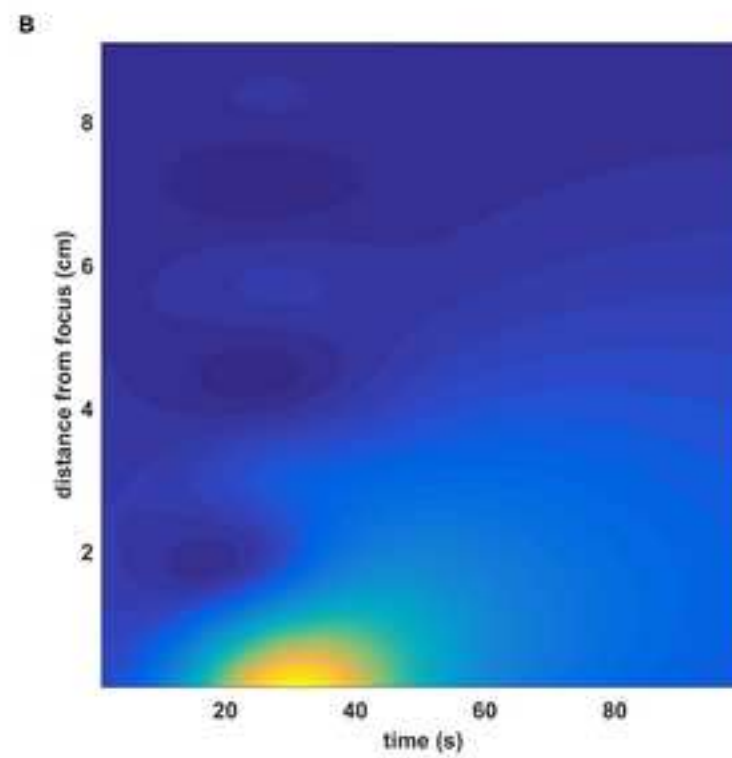
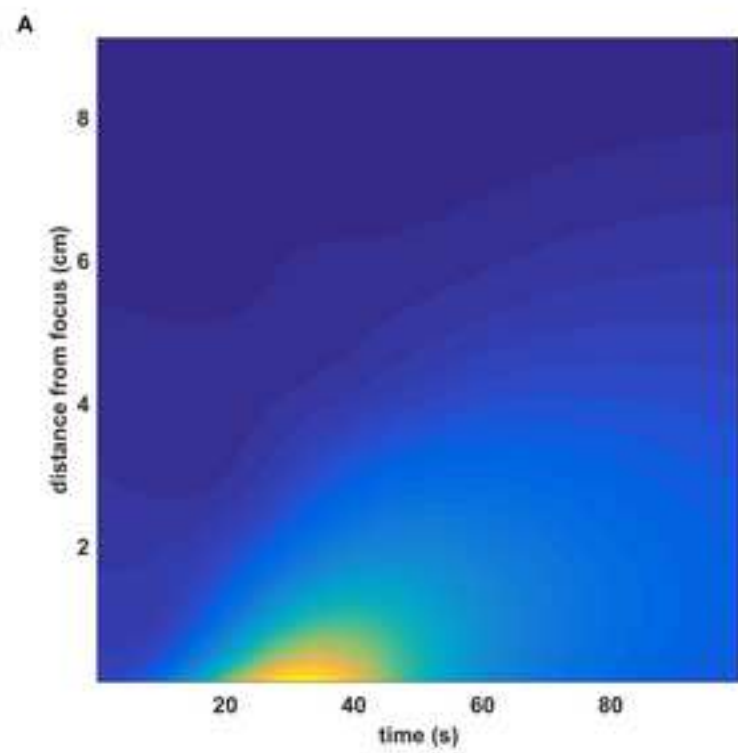


9. Figure 4
[Click here to download high resolution image](#)

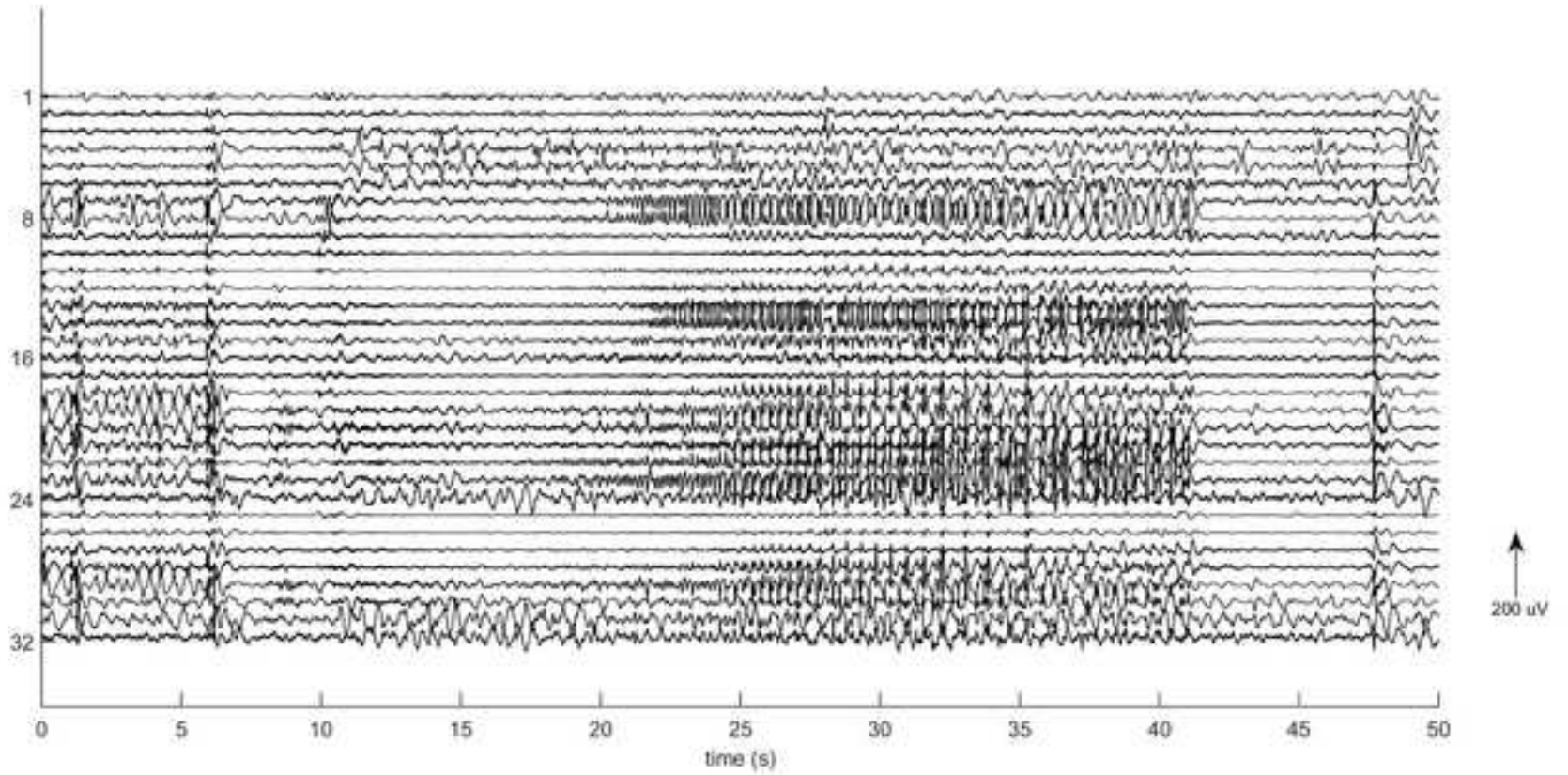


9. Figure 5

[Click here to download high resolution image](#)

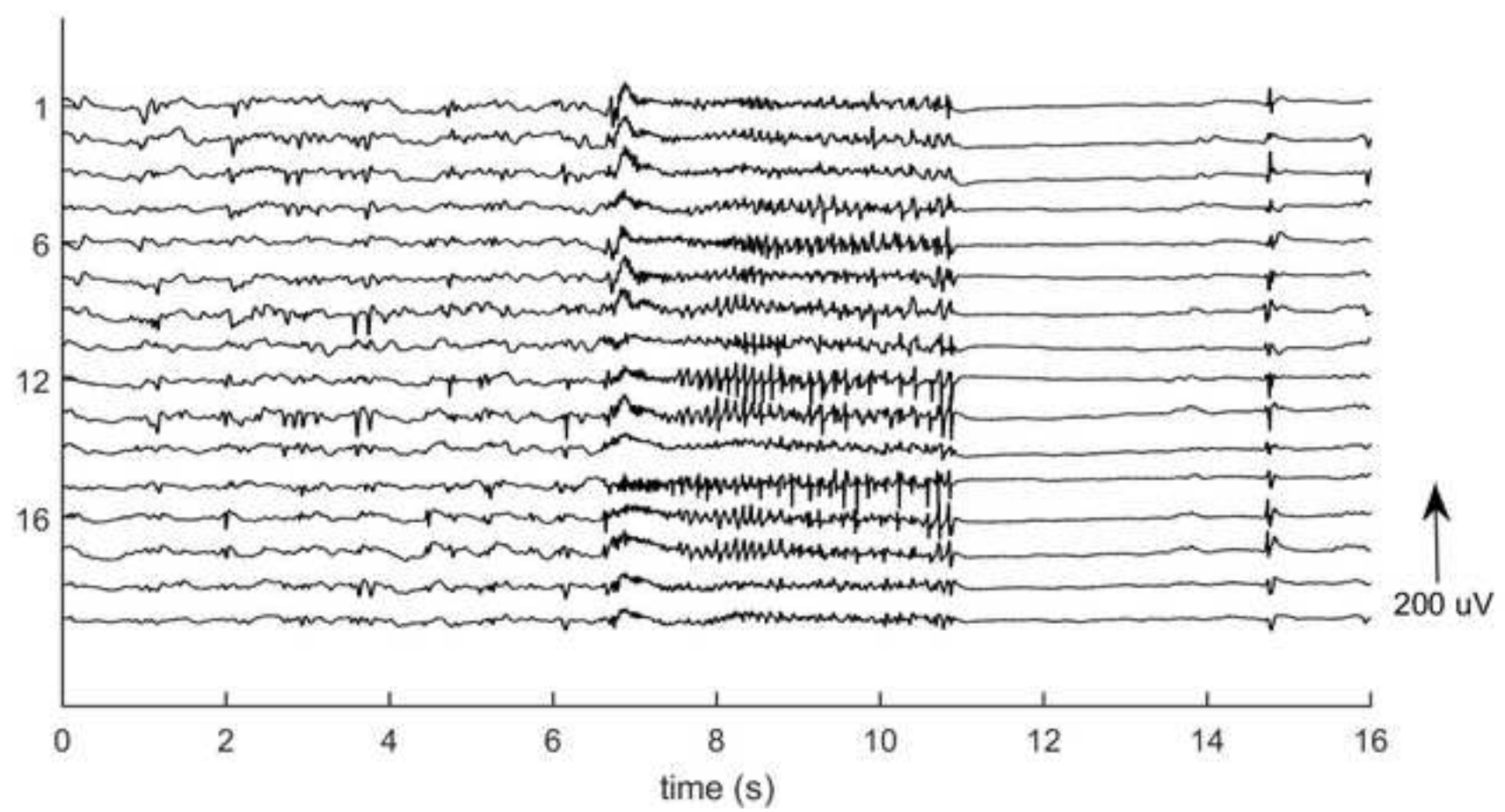


9. Figure 6
[Click here to download high resolution image](#)

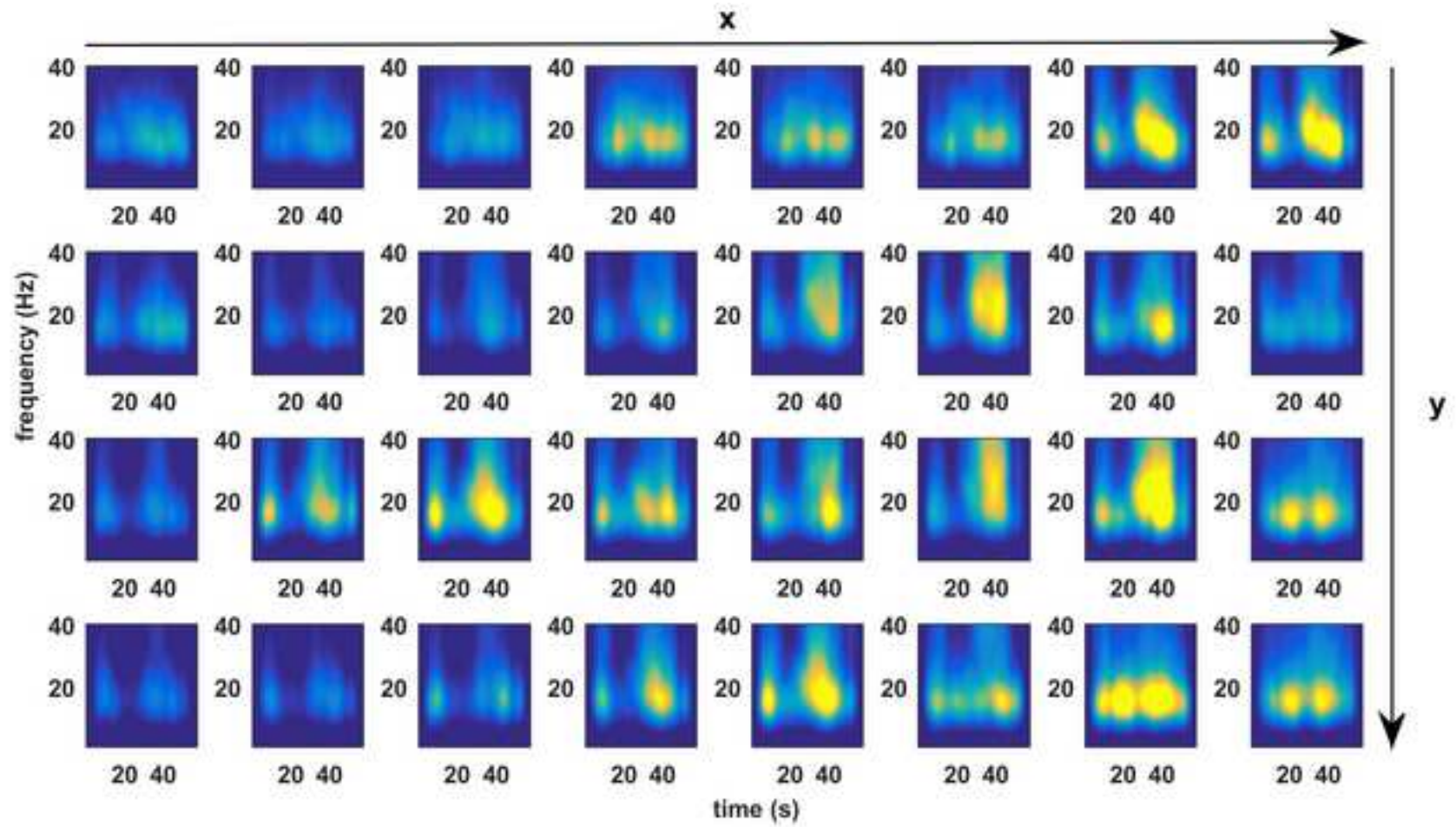


9. Figure 7

[Click here to download high resolution image](#)

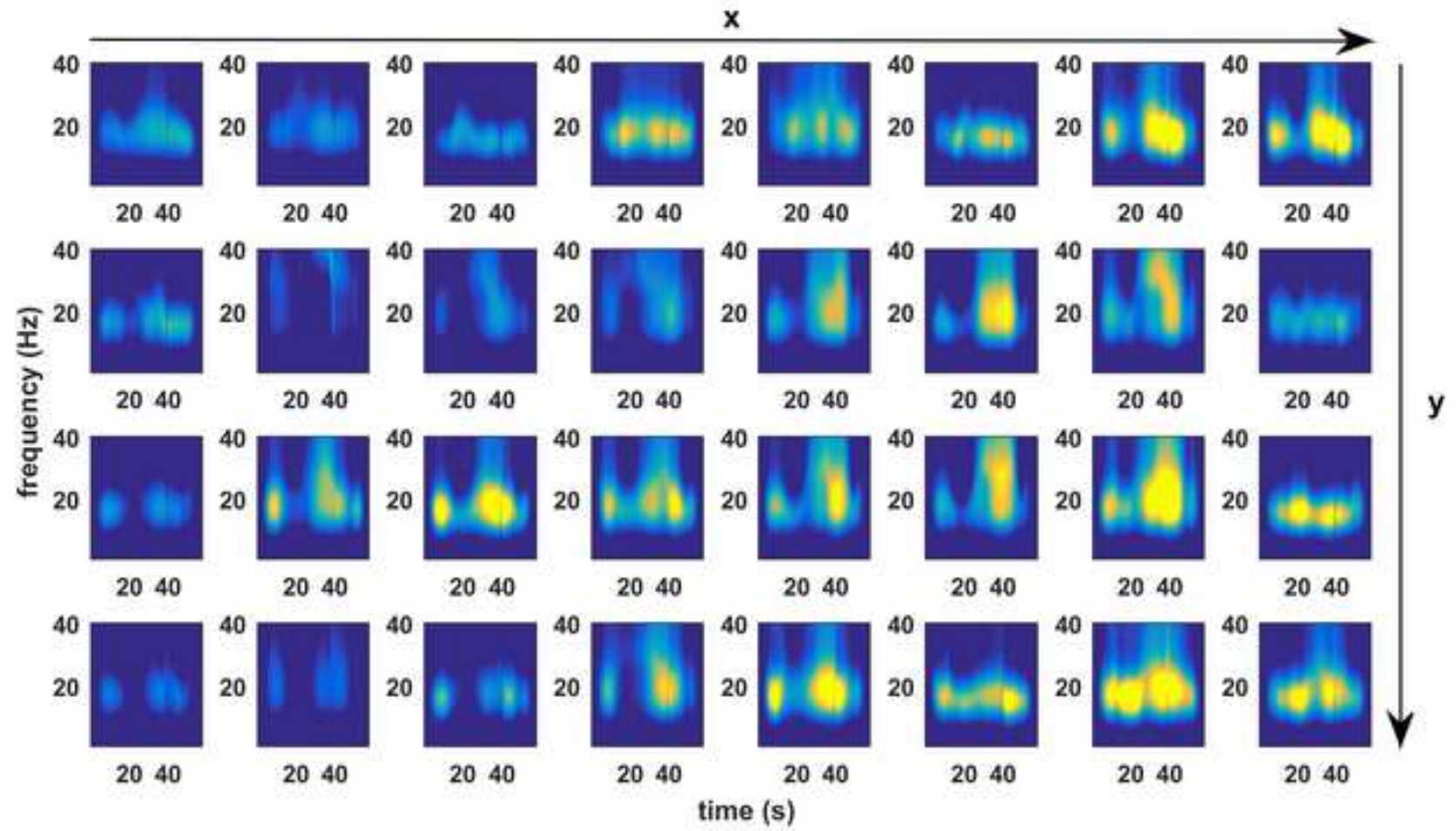


9. Figure 8
[Click here to download high resolution image](#)

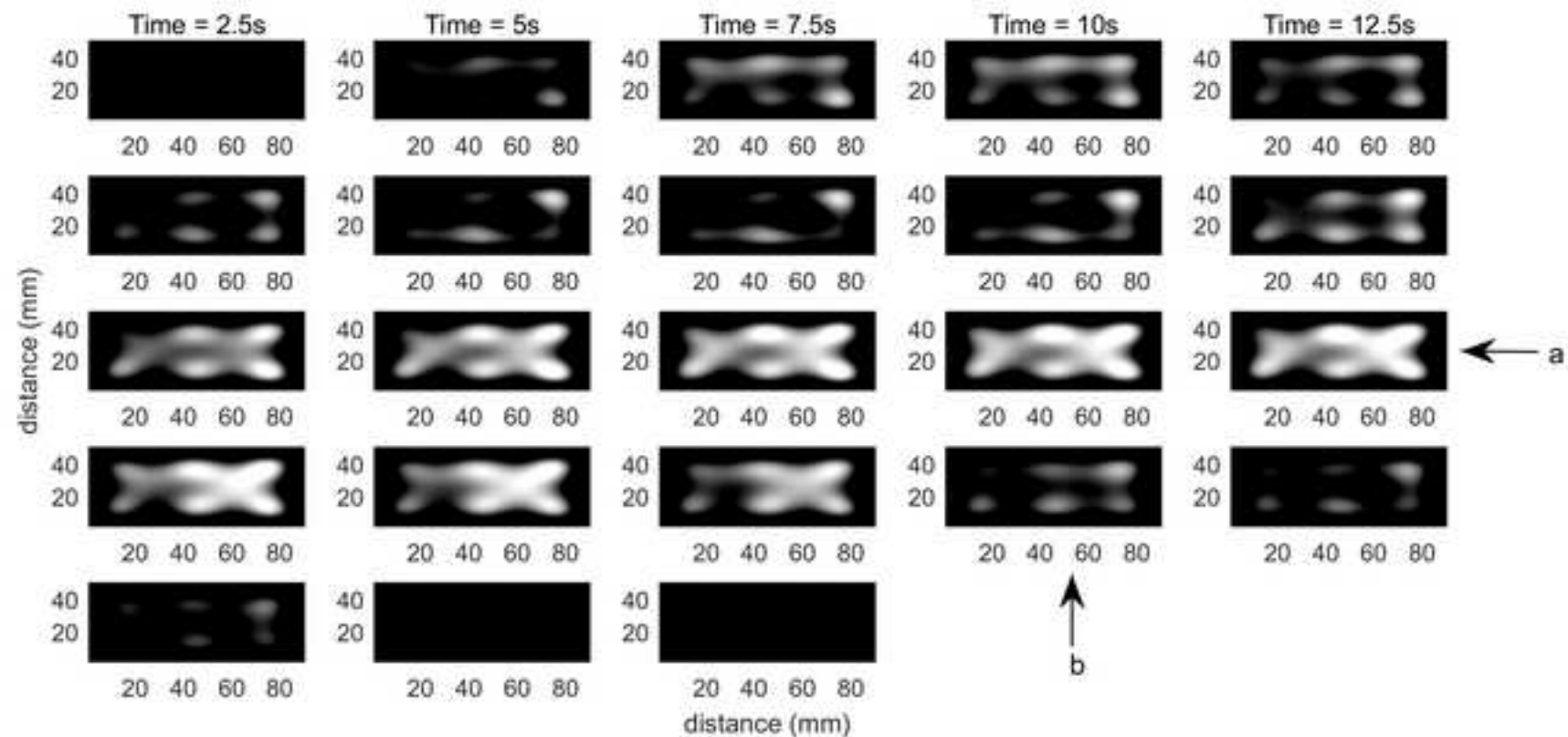


9. Figure 9

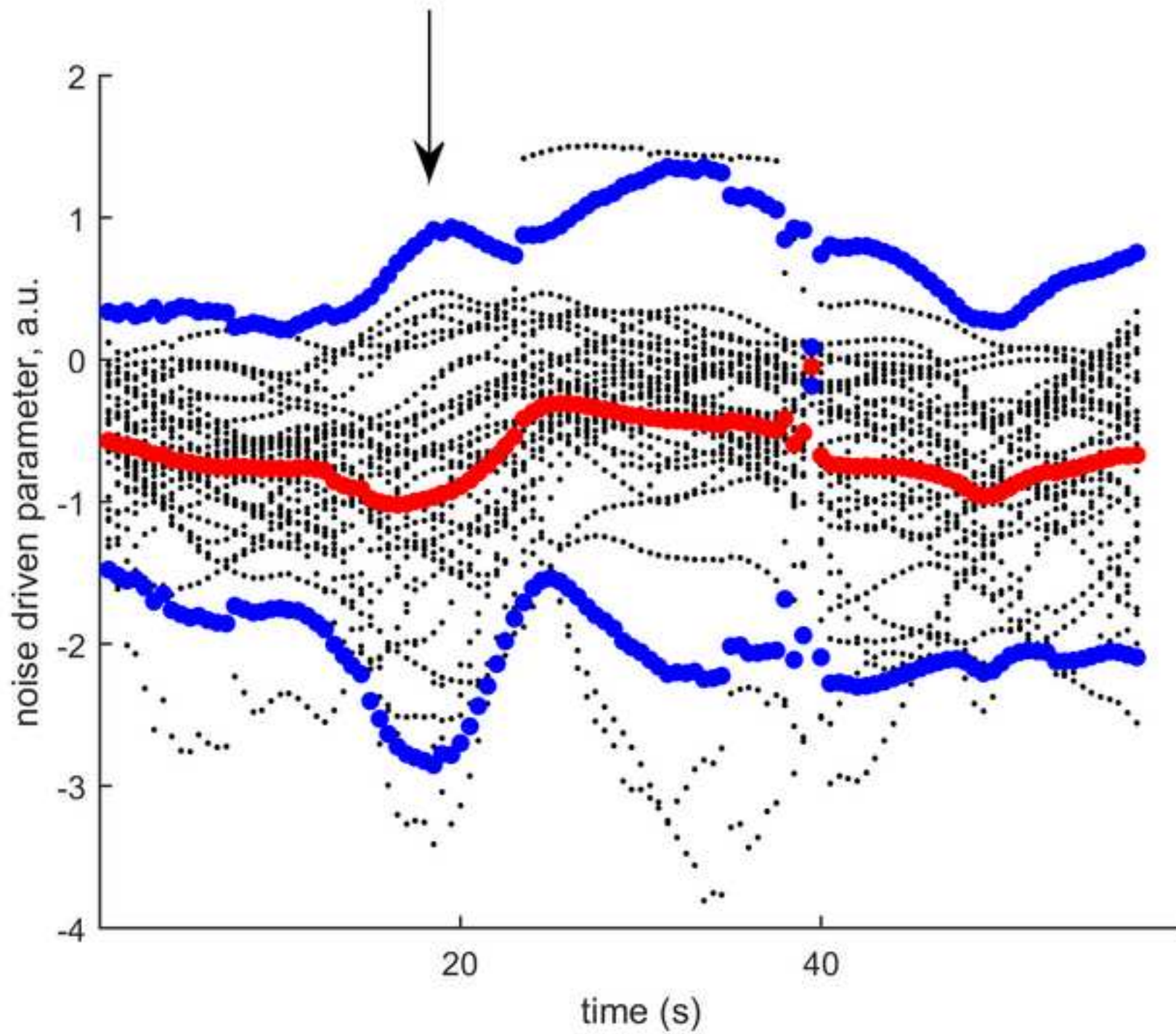
[Click here to download high resolution image](#)



9. Figure 10
[Click here to download high resolution image](#)

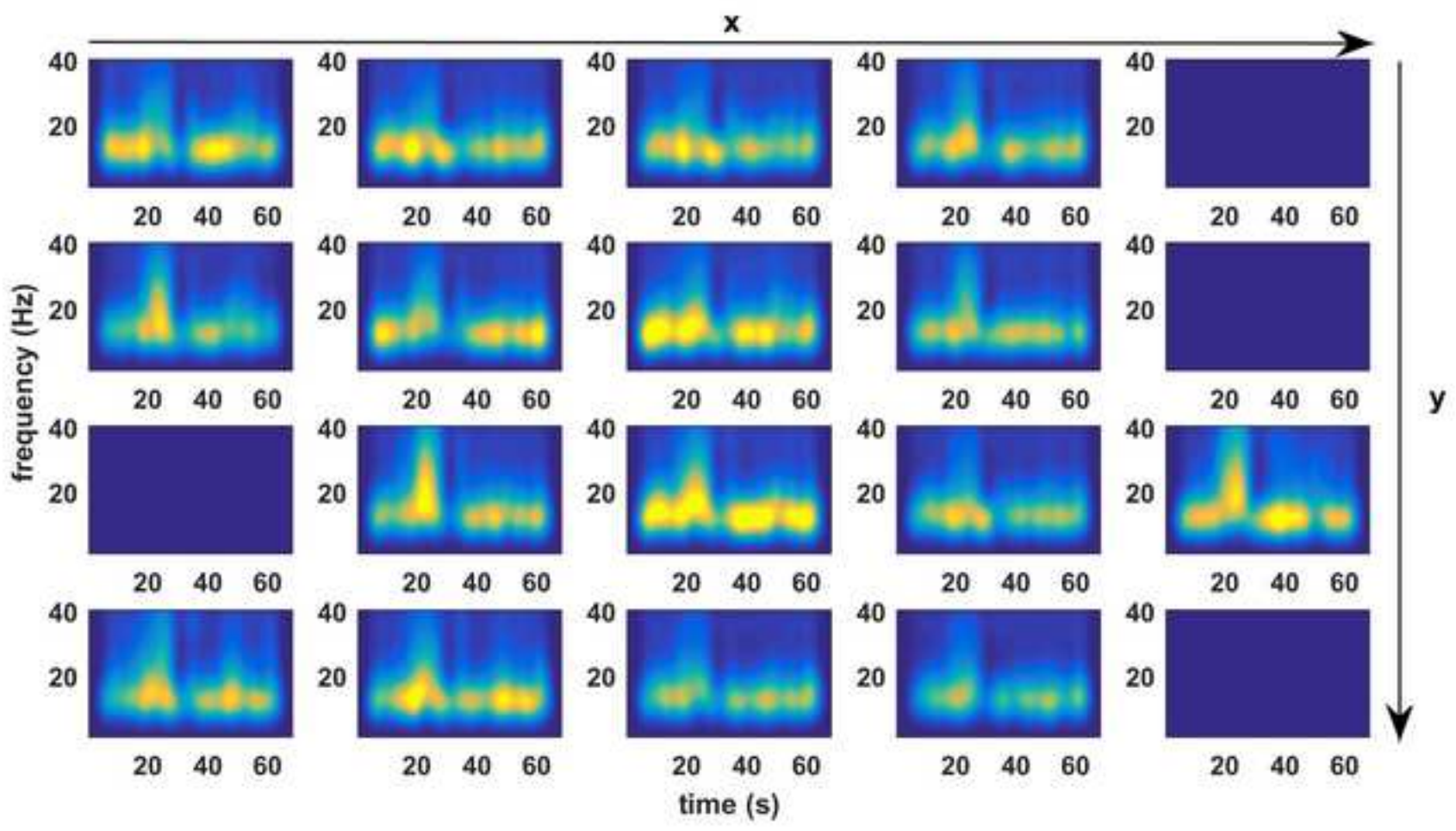


9. Figure 11
[Click here to download high resolution image](#)

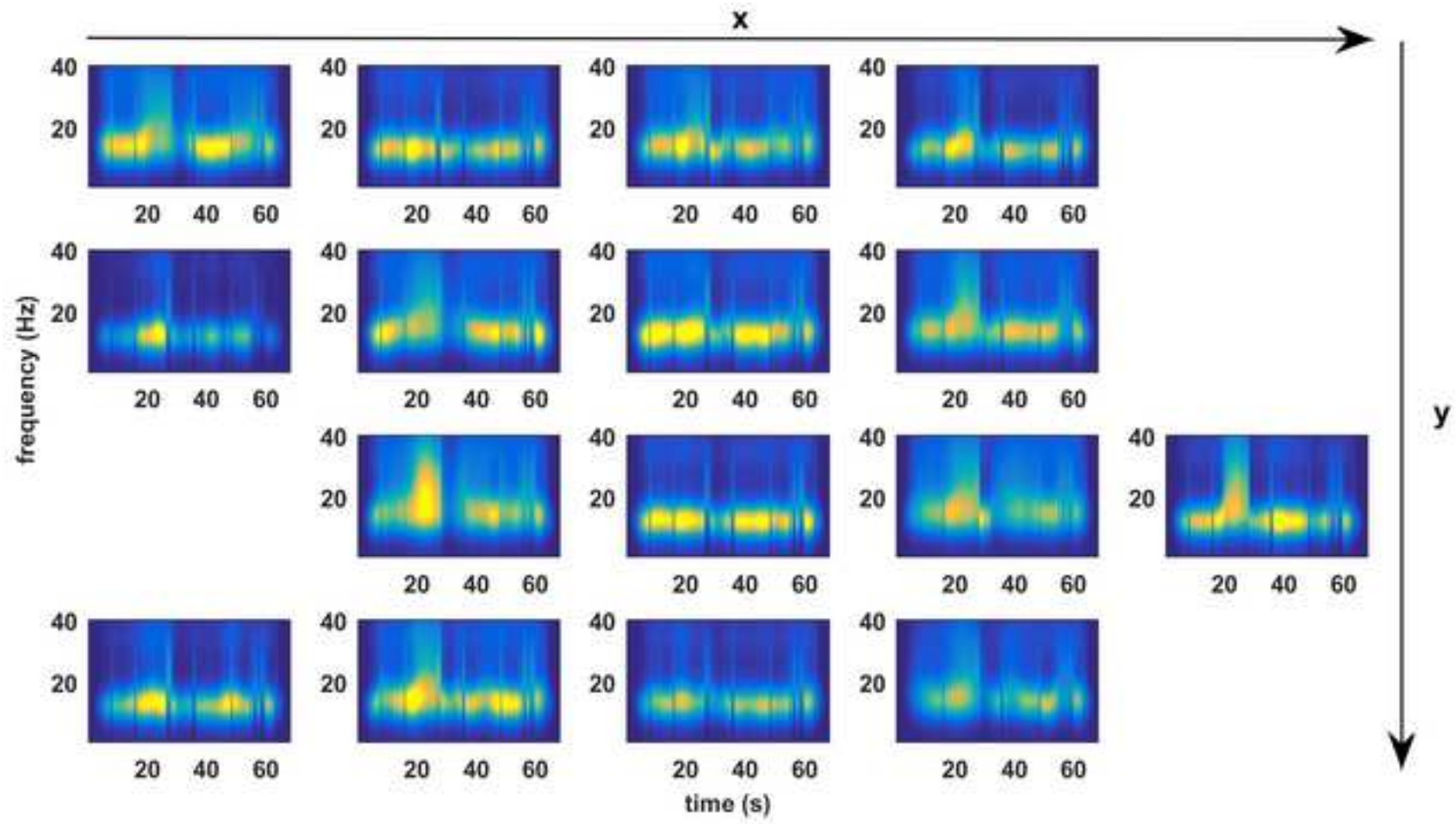


9. Figure 12

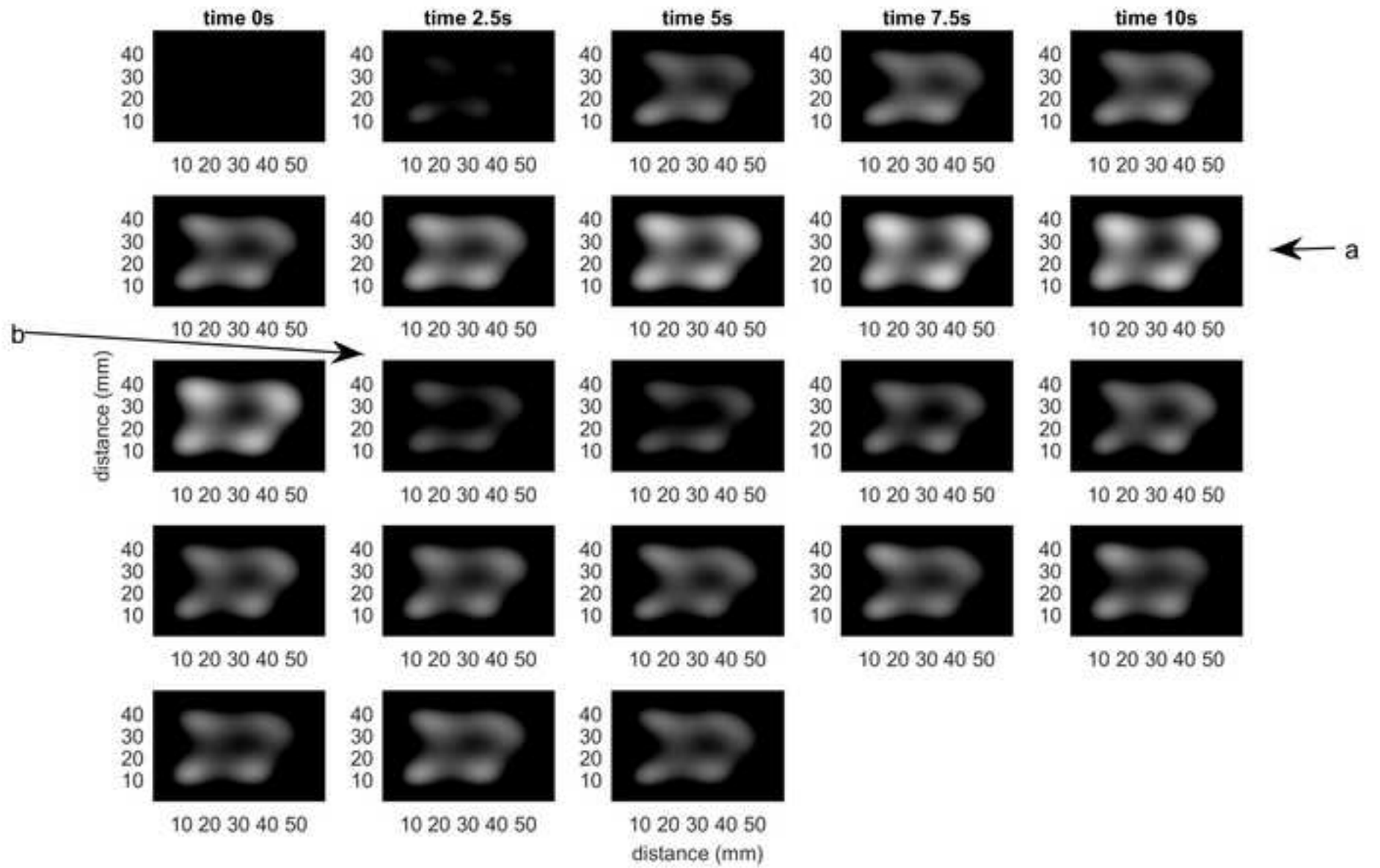
[Click here to download high resolution image](#)



9. Figure 13
[Click here to download high resolution image](#)

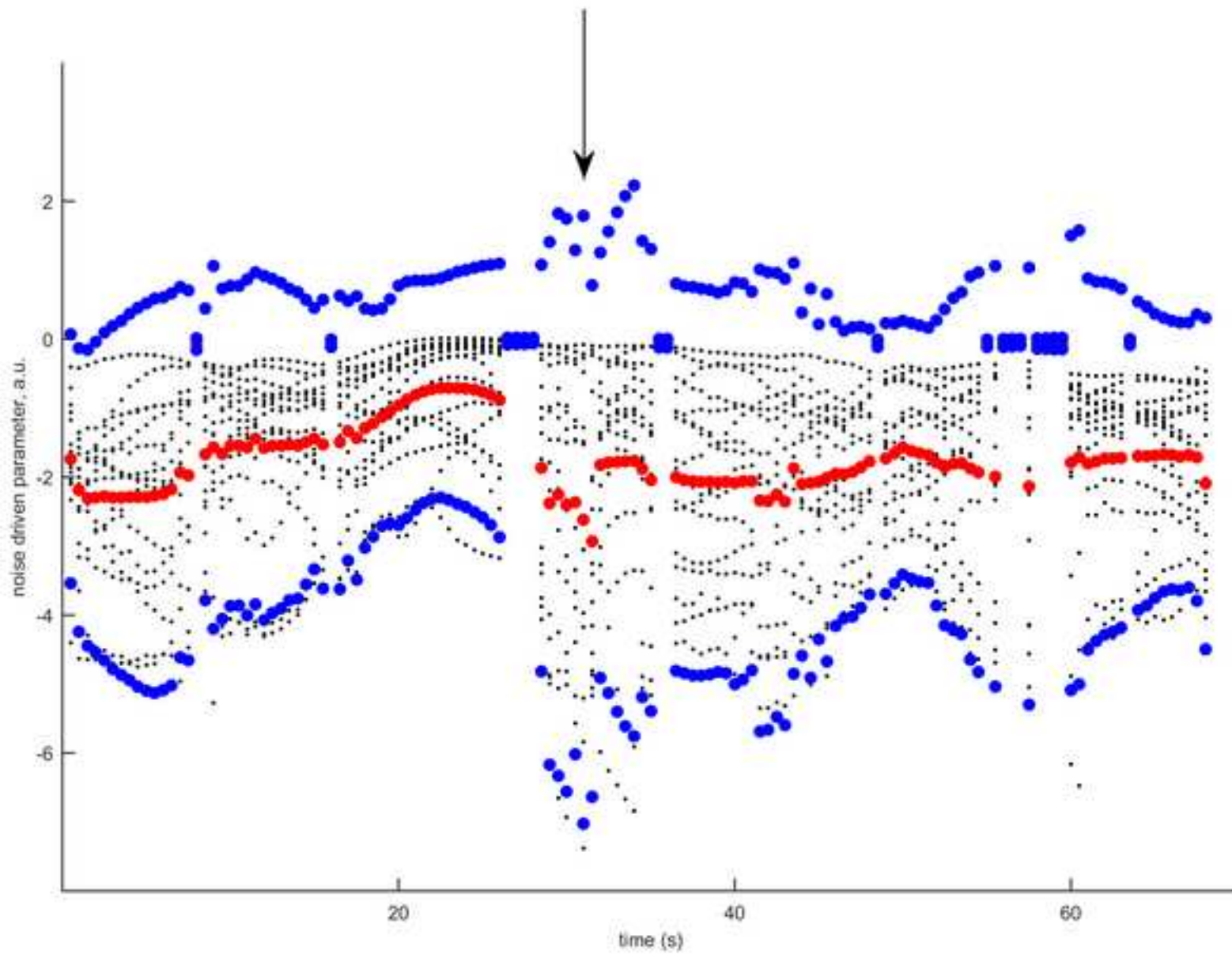


9. Figure 14
[Click here to download high resolution image](#)



9. Figure 15

[Click here to download high resolution image](#)



9. Figure 16
[Click here to download high resolution image](#)

